AFRL-AFOSR-UK-TR-2016-0008

Window for optimal frequency operation and reliability of 3DEG and 2DEG channels for oxide microwave MESFETs and HFETs

Arvydas Matulionis
CENTER FOR PHYSICAL SCIENCES AND TECHNOLOGY STATE SCIENTIFIC RESEARCH INSTITUTE

04/01/2016
Final Report

Air Force Research Laboratory
AF Office Of Scientific Research (AFOSR)/ IOE
Arlington, Virginia 22203
Air Force Materiel Command

REPORT DOCUMENTATION PAGE

Form Approved
OMB No. 0704-0188

1. REPORT DATE *(DD-MM-YYYY)*	2. REPORT TYPE	3. DATES COVERED *(From - To)*
09/28/2015	Final	13-Sep-2012 to 11-Sep-2015

4. TITLE AND SUBTITLE
Window for optimal frequency operation and reliability of 3DEG and 2DEG channels for oxide microwave MESFETs and HFETs

5a. CONTRACT NUMBER
FA8655-12-1-2109

5b. GRANT NUMBER
Grant 122109

5c. PROGRAM ELEMENT NUMBER
61102F

6. AUTHOR(S)
Matulionis, Arvydas

5d. PROJECT NUMBER

5e. TASK NUMBER

5f. WORK UNIT NUMBER

7. PERFORMING ORGANIZATION NAME(S) AND ADDRESS(ES)
CENTER FOR PHYSICAL SCIENCES AND TECHNOLOGY STATE SCIENTIFIC RESEARCH INSTITUTE, SAVANORIU 231, VILNIUS, , 02300, LT

8. PERFORMING ORGANIZATION REPORT NUMBER

9. SPONSORING/MONITORING AGENCY NAME(S) AND ADDRESS(ES)
EOARD
Unit 4515
APO AE 09421-4515

10. SPONSOR/MONITOR'S ACRONYM(S)
AFRL/AFOSR/IOE (EOARD)

11. SPONSOR/MONITOR'S REPORT NUMBER(S)
AFRL-AFOSR-UK-TR-2015-XXXX

12. DISTRIBUTION/AVAILABILITY STATEMENT
Distribution A: Approved for public release; distribution is unlimited.

13. SUPPLEMENTARY NOTES

14. ABSTRACT
This was a study of hot-electron transport, noise, and energy relaxation for doped zinc-oxide and structured ZnO transistor materials with a 2-D electron gas (2DEG) channel subjected to a strong electric field. We conclude that the ZnO 3DEG and 2DEG channels can be operated at the electron density window with better performance than at the off-window electron densities. Models based on the Boltzmann kinetic equation for hot electrons fail to interpret the experimental results unless hot-phonon accumulation is taken into account; assumption of electron density-independent hot-phonon lifetimes explains the transition of the hot electron-hot phonon system from weak to intense coupling but fails to predict window position.

15. SUBJECT TERMS
EOARD, MESFET, HFET, oxide microwave

16. SECURITY CLASSIFICATION OF:			17. LIMITATION OF ABSTRACT	18. NUMBER OF PAGES	19a. NAME OF RESPONSIBLE PERSON
a. REPORT	b. ABSTRACT	c. THIS PAGE			PUTZ, VICTOR
					19b. TELEPHONE NUMBER *(Include area code)*
Unclas	Unclas	Unclas	SAR	41	235-6013

Semiconductor Physics Institute
of
Center for Physical Sciences and Technology

AWARD NO. FA8655-12-1-2109
EUROPEAN OFFICE OF AEROSPACE RESEARCH AND DEVELOPMENT

Window for optimal frequency operation and reliability of 3DEG and 2DEG channels for oxide microwave MESFETs and HFETs

September 2012–September 2015

Final Report
Vilnius 2015

List of Coauthors

H. Morkoç
Ü. Özgur
V. Avrutin
H. Liu
N. Izyumskaya
M. Toporkov
J. Liberis
M. Ramonas
E. Šermukšnis
L. Ardaravičius
A. Šimukovič

Principal Investigator Arvydas Matulionis
Semiconductor Physics Institute of Center for Physical Sciences and Technology, Vilnius, Lithuania

Table of Contents

List of Tables

List of Figures

Figure 11. Dependence of excess noise temperature on supplied power per electron. Symbols stand for samples #567 (black), # 639 (blue), and #663 (red). Please see Table 1 for sample nomenclature. Black lines stand for linear dependence.

Figure 12. Slope of power-dependent excess noise temperature for several chips. Voltage pulse duration is 2.7 μs.

Figure 13. Density-dependent slope of power-dependent excess noise temperature over background temperature (symbols). Black curve guides the eye.

Figure 14. Hot-electron energy relaxation time for ZnO. Blue circles – present project [22], bullets worldwide results measured by photoexcitation techniques [8-20]. Dotted curve is semi-empirical dependence [36]. Solid curve guides the eye.

Figure 15. Dependence of hot-electron energy relaxation time on electron density for doped ZnO. Inset illustrates paths for hot-electron energy relaxation. Red line is Eq. (4) (path 1), blue line is Eq. (5) (path 2). Black line is Eq. (3) for the combined effect (paths 1 and 2) .

Figure 16. Monte Carlo simulation of hot-electron energy relaxation time for doped ZnO when hot-phonon effect is ignored (green symbols and curve). Blue circles are experimental data. Black line is Eq. (3) for the combined effect (paths 1 and 2).

Figure 17. Dependence of electron energy autocorrelation function on the time delay. Closed symbols represent the Monte Carlo data with hot-phonon effect at different electron gas density: $1 \bullet 10^{17}$ cm^{-3} (black squares), $3 \bullet 10^{17}$ cm^{-3} (blue stars), $5 \bullet 10^{17}$ cm^{-3} (red circles), $1 \bullet 10^{18}$ cm^{-3} (green triangles). Open triangles ignore hot phonon effect when the Monte Carlo simulation is performed for electron gas density of $1 \bullet 10^{18}$ cm^{-3}.

Figure 18. Monte Carlo simulation of density-dependent hot-electron energy relaxation time for doped ZnO. Open circles represent Monte Carlo data with hot-phonon effect taken into account (τ_{ph}= 3 ps is assumed, dashed line). Solid curve guides the eye.

Figure 19. Coupling index of hot-electron and hot-phonon gases.

Figure 20. Experimental dependence of hot-phonon lifetime on electron density for doped ZnO at room temperature (green symbols). Blue symbols stand for hot-electron energy relaxation time. Lines guide the eye.

Figure 21. Experimental dependence of hot-phonon lifetime on electron density for doped ZnO (green stars, present project) and nominally undoped GaN (black squares, [33]). Black line stands for theoretic model of decay of coupled plasmon–LO-phonon modes [37]. Green line guides the eye.

Figure 22. Experimental dependence of hot-electron drift velocity on electron density for doped ZnO (symbols, present project). Lines guide the eye. Data at high fields for high-density channels are missing because of thermal runaway. Voltage pulse duration 1.5 ns.

Figure 23. Dependence of excess hot-electron noise for 2DEG channel located in $ZnO/Mg_{0.38}Zn_{0.62}O/ZnO$ structure. Line is drawn for τ_{ph} =55 fs. [23]

Figure 24. Hot-phonon lifetime in 2DEG channels located in $ZnO/Mg_{0.38}Zn_{0.62}O/ZnO$ structure (green star, present project) together with the data for 2DEG channels confined in GaN (black bullets [7], blue star [39], red triangle [41]), InGaAs (red circles [7]) and InGaN (blue square [40]). Solid curves illustrate Eq. (5).

Publications

E. Šermukšnis, J. Liberis, M. Ramonas, A. Matulionis, M. Toporkov, H. Y. Liu, V. Avrutin, Ü. Özgür, and H. Morkoç, Hot-electron energy relaxation time in Ga-doped ZnO films**,** *Journal of Applied Physics* **117**, 065704 (2015) (8pp).

E. Šermukšnis, M. Ramonas, J. Liberis, A. Matulionis, V. Avrutin, H. Liu, N. Izyumskaya, Ü. Özgür, H. Morkoç, Electron energy relaxation in wurtzite ZnO and GaN, *Proc. ICNF* **22**, in Proc. IEEE DOI:10.1109/ICNF.2013.6578917 (4pp).

E. Šermukšnis, J. Liberis A. Matulionis, M. Toporkov, V. Avrutin, Ü. Özgür, H. Morkoç, Hot–electron noise and energy relaxation in wurtzite ZnO, *Proc. ICNF* **23**, 1570080493 (2015) (4pp).

E. Šermukšnis, J. Liberis, A. Matulionis, V. Avrutin, R. Ferreyra, Ü. Özgür, H. Morkoç, „Hot-electron real-space transfer and longitudinal transport in dual AlGaN/AlN/{AlGaN/GaN} channels“ *Semiconductor Science and Technology,* **30**, 035003 (2015) (6 pp).

Reports

1. Arvydas Matulionis, ***Window for optimal performance of doped ZnO channels,*** AFOSR Project FA8655-09-1-2109 Oral half-annual report, Arlington, February 21, 2013; VCU, Richmond, February 22, 2013.

2. E. Šermukšnis, M. Ramonas, J. Liberis, A. Matulionis, V. Avrutin, H. Liu, N. Izyumskaya, Ü. Özgür, H. Morkoç, ***Electron energy relaxation in wurtzite ZnO and GaN***, oral report at the 22nd International Conference on Noise and Fluctuations (ICNF-2013) Montpellier, France, June 24th to June 28th, 2013.

3. E. Šermukšnis, J. Liberis, A. Matulionis, M. Toporkov, H. Liu, V. Avrutin, N. Izyumskaya, Ü. Özgür, H. Morkoç, Electron Energy Relaxation Time in n-Type Wurtzite ZnO, oral report at the 8th International Workshop on Zinc Oxide and Related Materials (IWZnO 2014) September 7-11, 2014 Niagara Falls, Ontario, Canada.

4. Emilis Šermukšnis, ***Window for optimal performance of doped ZnO channels,*** AFOSR Project FA8655-09-1-2109 Oral annual report, VCU Richmond, September 19, 2013.

5. E. Šermukšnis, J. Liberis A. Matulionis, M. Toporkov, V. Avrutin, Ü. Özgür, H. Morkoç, ***Hot–electron noise and energy relaxation in wurtzite ZnO***, oral report at the 22nd International Conference on Noise and Fluctuations (ICNF-2015) Xi'an, China, June 8th to June 12th, 2015.

Summary

Hot-electron transport, noise, and energy relaxation were investigated in donor-doped bulk wurtzite ZnO (epitaxial layer form) and a $ZnO/Mg_{0.38}Zn_{0.62}O/ZnO$ structure with a two-dimensional electron gas (2DEG) channel subjected to a strong electric field. Ga-doped and Sb-doped gateless ZnO channels contained electron density in the range from $1.4 \cdot 10^{17}$ cm^{-3} to $1.3 \cdot 10^{20}$ cm^{-3}. The electron sheet density in the 2DEG channel was $5.5 \cdot 10^{12}$ cm^{-2}. Non-equilibrium longitudinal optical phonons (hot phonons) were found to play an essenetial role. Plasmon-assisted decay of hot phonons supported enhanced electron drift velocity, fast relaxation of electron energy, and reduced hot-electron noise in the electron density window situated in the vicinity of plasmon–LO-phonon resonance.

The nanosecond pulsed measurements yielded hot-electron drift velocity in agreement with those of the Monte Carlo simulation when the density of the ionized impurities is allowed to exceed that of the electrons by 10–13 times in bulk ZnO. The Ohm law approximately holded in the electric field range up to 100 kV/cm at an electron density of $1.42 \cdot 10^{17}$ cm^{-3} but the range shrinked at higher electron densities. The non-ohmic behavior caused by increase in the background temperature represented by acoustic phonons. A drift velocity of $1.5 \cdot 10^{7}$ cm/s was measured at 104 kV/cm field.

The electronic noise was investigated experimentally in doped ZnO epitaxial layers subjected to pulsed electric field at room temperature and used to interpet hot-electron energy relaxation. The noise spectral measurements at 0.2 GHz–2.5 GHz frequencies suggested that the hot-electron noise dominated over generation–recombination and 1/f sources at 10 GHz, and the noise at (and above) this frequency was treated in terms of hot-electron temperature. The extracted hot-electron energy relaxation time depended on the electron density. The relaxation time increased from 0.17 ps to 1.8 ps when the electron density increased from $1.4 \cdot 10^{17}$ cm^{-3} to $1.3 \cdot 10^{20}$ cm^{-3}. The local minimum was resolved near the electron density of $1.4 \cdot 10^{19}$ cm^{-3}. A systematic dependence of the relaxation time on the electron density was measured for the donor-doped ZnO for the first time.The longest energy relaxation time (1.8 ps) was in a reasonably good agreement with the published values obtained through optical time-resolved luminescence and absorption experiments.

The Boltzmann kinetic equation for hot electrons failed to interpret the experimental results unless hot-phonon accumulation was taken into account. The assumption of electron density-independent hot-phonon lifetime led to a monotonous increase in the hot-electron energy relaxation time. This proved the transition of the hot-electron–hot-phonon system from the weak coupling regime to the intense coupling regime. The results of Monte Carlo simulation for density-independent hot-phonon lifetime were in a qualitative agreement with the experimental data except for the local minimum resolved at the electron density of $1.4 \cdot 10^{19} cm^{-3}$. The local minimum was associated with the plasmon-assisted rapid decay of hot phonons as demonstrated earlier for nitride and arsenide two-dimensional channels.

The hot-electron noise measurements at 38.5 GHz demonstrated ultrafast relaxation of the hot-electron energy in the 2DEG channel confined in the $ZnO/Mg_{0.38}Zn_{0.62}O/ZnO$ structure. The relaxation time of 55 fs was extracted at a 2DEG density of $5.5 \cdot 10^{12}$ cm^{-2}. This ultrafast relaxation occurs in the vicinity of LO-phonon–plasmon resonance. The comparative analysis of the results for the 2DEG channels located in ZnO, GaN, InGaN, and InGaAs led to the conclusion that the dissipation was enhanced by plasmons. The results were in good agreement with those obtained for the doped ZnO films.

1. Introduction

Wide band-gap semiconductor transistors are considered as imperative for critical platforms in microwave communication systems, radars, electromagnetic testing, and military systems for reconnaissance, weapons control, patrol, and intelligence operations. Traditional diamond, silicon carbide, and nitride field-effect transistors (FETs) operate at microwave and millimeter-wave frequencies with success; their main drawback is the lack of high quality, large area, lattice-matched, and inexpensive substrates for epitaxial growth of heterostructures with a high-density two-dimensional electron gas (2DEG) confined in a quantum well situated in the high-purity semiconductor. A promising alternative comes from II-VI chalcogenides (CdS, ZnS) and oxides (ZnO, CdO, MgO, BeO) and their heterostructures grown on native substrates [1-3]. Expected high structural quality promises efficient operation of ZnO FETs and ZnO/MgZnO heterostructure field-effect transistors (HFETs) at centimeter and millimeter-wave frequencies [4].

Fast relaxation of hot electrons is a prerequisite for transistor performance at high frequencies. The supplied electric power is dissipated mainly through electron coupling with LO phonons, while the secondary role is played by elastic ionized impurity scattering and quasi-elastic acoustic phonon scattering. The high-field electron transport is accompanied with intense LO-phonon emission by hot electrons, and the emitted non-equilibrium LO phonons accumulate. The associated phenomena are often referred to as hot-phonon effects. In general, hot phonons are important for devices operated at high electric fields, such as microwave and high power field-effect transistors, because of the pivotal role they play in heat dissipation and device reliability [5]. Very short LO-phonon lifetimes are desirable for reliable operation of the transistor channel. Strong coupling of the hot phonons with the electrons causes the desired fast electron energy relaxation if the hot-phonon decay is fast. The fastest decay of hot phonons takes place in the vicinity of plasmon–LO-phonon resonance [6]. The plasmon involvement paves the way for the electron density window where transistors exhibit the fastest operation, the lowest phase noise, and the slowest device degradation as demonstrated for GaN HFETs [7]. A similar window has not yet been determined through experiments on ZnO transistors. The window can be resolved through experiments on noise and hot-electron energy relaxation. Based on GaN HFET data, the window for ZnO is expected at the optimal electron density for the resonant plasmon-assisted decay of hot phonons. According to a model of infinite uniform plasma, the plasmon–LO-phonon resonance is expected at $6.8 \cdot 10^{18}$ cm^{-3} in bulk ZnO. However, the resonance density is higher in thin channels because the plasma frequency decreases together with the channel thickness.

Figure 1 illustrates the results on hot-electron energy relaxation time measured by optical techniques [8–20]. A large body of the experimental data lies near 1 ps. Some data points deviate from the main group in a random manner, but a systematic dependence on electron density is not resolved.

This project aims at resolving the electron density window for the fastest decay of hot phonons in ZnO through measuring hot-electron energy relaxation. Hot-electron noise technique is the most suitable for achieving the goal. Doped ZnO is a good alternative as compared with the investigated nominally undoped ZnO where the electron density is varied by photoexcitation. Doping is preferable for several reasons: (i) a high-density electron gas is present at equilibrium, (ii) doped channels are of direct interest for FETs, (iii) doping assures uniformity of the electron gas, (iv) the gas density is fixed (while the photoexcited electron–hole pairs are distributed in a depth-dependent manner in optical pump–probe experiments and, in addition, the density depends on time).

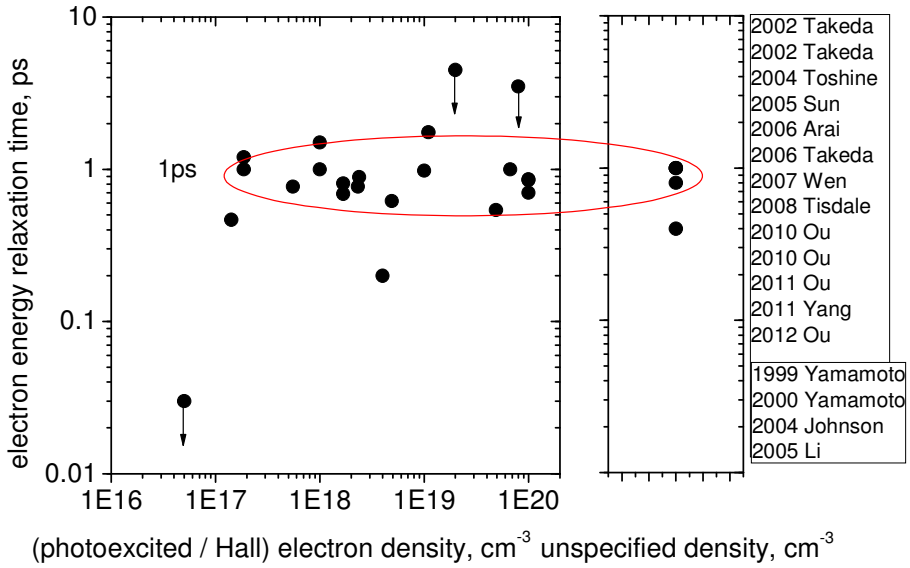

Figure 1. Hot-electron energy relaxation time for ZnO measured by photoexcitation techniques [8-20].

As noted above, this project deals with the hot-electron transport and noise in the doped ZnO channels subjected to strong electric field. The unsolved problem of electron density window in ZnO channels is discussed in the Introduction. Section 2 presents the techniques for measurement of hot-electron effecs. The main attention is paid to the fluctuation–dissipation technique for the hot-electron energy relaxation time. The results on hot-electron drift velocity are compared with those of Monte Carlo simulations in Section 3. Section 4 presents the experimental results on the doping-dependent excess noise. The hot-electron energy relaxation time is extracted from the noise measurements and compared with the available data in Section 5. Section 6 discusses the experimental results together with those of Monte Carlo simulation of the hot-electron energy correlation functions in terms of hot-phonon effects. The resonant behavior is associated with plasmon-assisted decay of hot phonons. The ultrafast decay of hot phonons in 2DEG channels is discussed in section 7. The report ends with the main conclusions. For readers' convenience a list of abbreviations and symbols is attached.

2. Methods, Assumptions, and Procedures

2.1. Samples

The investigated samples were grown and processed at Virginia Commonwealth University by the group of Prof. H. Morkoç. The ZnO films were grown on a-plane sapphire substrates by plasma-enhanced molecular beam epitaxy (PMBE). Plasma power of 400 W was used for depositing of the films. The growth of the ZnO films was monitored by in situ reflection high energy electron diffraction. A 5-nm-thick low-temperature ZnO buffer layer was deposited at 300°C for enhanced nucleation and

annealed at 700°C prior to the growth of doped ZnO layer. The layer thickness was 150–350 nm. Structural properties and surface morphology were studied by X-ray diffraction, transmission electron microscopy, and atomic force microscopy. Electron density and mobility in the doped channel were assessed by Hall measurements performed in the van der Pauw configuration with soldered indium contacts (Table 1). Coplanar Ti/Au (25 nm/50 nm) electrode patterns were defined through standard photolithography and lift-off procedure. Contact resistance was estimated from measurements of sample resistance as a function of channel length. Channels selected for noise measurements had the typical length of L=5.8 μm and the width of w = 250 μm.

Table 1. ZnO channel data.

Wafer	Dopant	Channel thickness, nm	Electron density, cm^{-3}
#567	Ga	330-340	$1.42 \cdot 10^{17}$
#570	Ga	350	$5.5 \cdot 10^{17}$
#571	Ga	350	$2.39 \cdot 10^{18}$
#639	Ga	300	$4.9 \cdot 10^{18}$
#753	Ga	200	$1 \cdot 10^{19}$
#751	Ga	200	$1.1 \cdot 10^{19}$
#661	Ga	150	$1.74 \cdot 10^{19}$
#487	Sb	170	$4.6 \cdot 10^{19}$
#663	Ga	225	$1.27 \cdot 10^{20}$

The ZnO/$Mg_{0.38}Zn_{0.62}O$/ZnO structures were grown on c-plane sapphire substrates by plasma-enhanced molecular-beam epitaxy. First, a 2-nm thick MgO layer was deposited at a substrate temperature T_S = 700°C followed by low-temperature ZnO deposited at T_S = 300°C and annealed at 700°C. Then a 100-nm ZnO buffer layer and a 130-nm MgZnO barrier were grown at 620°C and 350°C, respectively. The growth was finished by depositing a 40-to-50-nm thick ZnO channel layer at T_S = 620°C. Oxygen plasma cell operating at 400 W served as the source of reactive oxygen while Zn and Mg were evaporated from K-cells. The oxygen pressure in the growth chamber was $1.2 \cdot 10^{-5}$ Torr. The growth rates of the MgZnO and the high-temperature ZnO were 75 and 100 nm/h, respectively. For the noise measurements, patterns used in transmission line method (TLM) were fabricated by conventional photolithography followed by Ti/Au contact evaporation and lift-off process. The same TLMs were used for measurement of the contact resistance. The channel length of 15.8 μm was selected for the noise measurements. Because of large conduction band gap in MgZnO, the 2DEG is predominantly located in the top ZnO layer at the ZnO/MgZnO interface of the ZnO/MgZnO/ZnO structure. The 2DEG density is $5.5 \cdot 10^{12}$ cm^{-2}.

2.2. Pulsed Measurement of Noise Temperature

The hot-electron relaxation can be studied through noise measurements. The suitable fluctuation–dissipation technique has been developed and implemented after careful analyses of noise sources in voltage-biased semiconductors and 2DEG channels [21]. The hot-electron energy relaxation time can

be estimated under the main conditions: (i) the hot-electron velocity fluctuations cause the main source of excess noise, (ii) the background noise (represented mainly by acoustic phonon temperature) remains only weakly disturbed by the applied electric field. Caution should be exercised to ensure that the electric field is not sufficiently high to induce intervalley scattering and impact ionization with their complex noise signature.

The first condition is satisfied at sufficiently high frequencies where generation–recombination (G–R) noise and 1/f fluctuations do not manifest themselves. The thermal walkout of the background temperature can be minimized when the electrons are heated by pulsed voltage. The choice of pulse duration requires a compromise in that higher electric fields are applied if the pulses are shorter. In this case, gating pulses for noise integration must be short, and the sensitivity is compromised. Longer pulses (and longer integration gating) are used at relatively low fields and low electron densities, when the thermal walkout is of no concern.

In the present work the measurements are carried out on channels supplied with coplanar ohmic electrodes. The hot-electron fluctuations cause emission of microwave radiation (noise power) detected by a sensitive gated radiometer. The equivalent noise temperature, or simply noise temperature, is determined from the measured noise power. The measurements can be made before, during, and after the main voltage pulse used to heat the electrons. For this purpose the radiometer is opened by the gating pulse. Short pulses of the applied voltage allow one to control thermal walkout.

We used three different set-ups for measurement of the noise temperature in the frequency bands from 0.2 GHz to 2.5 GHz [22], in the X band in the vicinity of 10 GHz [21]), and in the vicinity of 38.5 GHz of the Ka band [23]. The sample is either mounted into the waveguide or accessed in an on-wafer mode. The noise temperature is measured in the bias direction. Microwave frequency range was found to be most suitable for the experimental study of hot-electron effects. The frequency of 10 GHz was high enough to suppress the G–R noise in the investigated doped ZnO channels [23]. However, the same did not hold for ZnO-based 2DEG channels, and the set-up for 38.5 GHz was developed [23].

The set-up for (0.2 – 2.5) GHz band is described in Ref. [22]. The pulse voltage generator is connected to the DUT (Fig. 2, 4) through a low-pass filter 2 (mini-circuit either BLP-1.9+ or BLP-5+) and a pulsed bias-tee 3 (Aeroflex 8860SFM2-02). The voltage pulse heats the electrons in the DUT. The noise emitted by the DUT passes through the pulsed bias-tee 3, the high-pass filter 5 (mini-circuit either SHP-25+ or BHP-250+), the RF bridge 7 (Eagle RLB150M5A), and is amplified by the low-noise amplifier 8 (Wenteq ABL0300-01-3414) up to the level appropriate for detection by the spectrum analyzer 9. We use a real time digital sampling oscilloscope (Agilent Infinium 54850) connected to a personal computer as a spectrum analyzer. The calibrated standard noise generator 6 (Agilent HP346C opt H01) serves as a reference source. The probe station and the RF probes are used for investigation in the on-wafer mode.

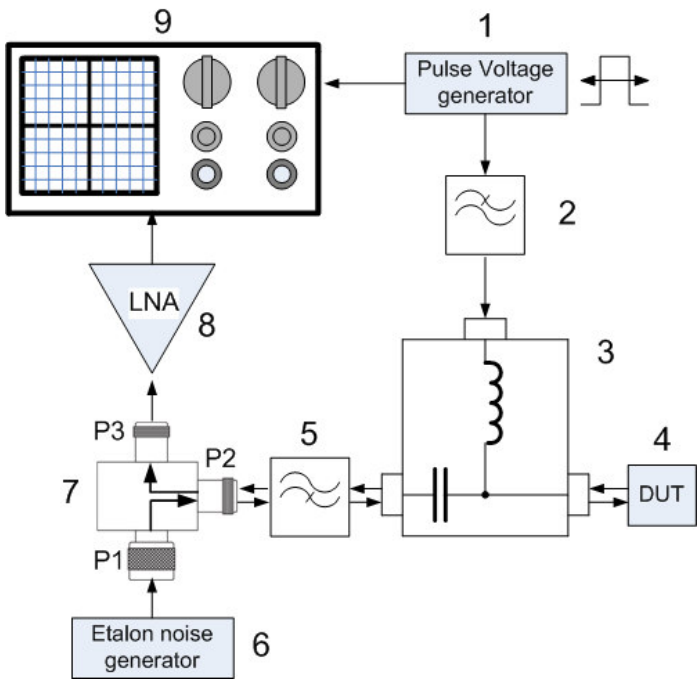

Figure 2. Pulsed noise spectrometer for 0.2 GHz – 2.5 GHz frequency band. 1 – pulsed voltage generator, 2 – low-pass filter, 3 – pulsed bias-tee, 4 – DUT, 5 – high-pass filter, 6 – standard noise source, 7 – RF bridge, 8 – low-noise amplifier , 9 – digital sampling oscilloscope [22].

Figure 3 presents a schematic block circuit of the gated radiometer. The X-band set-up includes JCA812 microwave low noise amplifiers and Stanford Research Systems modules (gated integrator and boxcar module SR250, Quad fast amplifier SR240A, and computer interface module SR245). Cascaded wideband (DC–350 MHz) SR240A amplifiers amplify the signal after the microwave detector before the gating. The noise power is digitized in the computer module SR245 and loaded through RS232 interface to the PC for further averaging. The computer integrates the noise power during the gating time and compares the result with the noise power of the standard source of noise. Each second value is inverted before the averaging, and the noise power difference is obtained. Hand-written Labview software controls the measurements and the data processing. Sample mismatch is taken into account. The measurements include four steps used to obtain the noise temperature and the sample reflection coefficient, for details see Ref. [22]. The thermal walkout is controlled through measurements before, during, and after the voltage pulse.

Recently the set-up for 38.5 GHz was developed [23] in order to investigate the hot-electron noise in ZnO-based 2DEG channels where the contribution of low-frequency sources could not be ignored at 10 GHz. The noise propagation path was designed for the Ka band. The band-pass filter selected a relatively narrow band with the 1 GHz bandwidth centered at frequency of 38.5 GHz. The rectified noise signal was integrated and converted to the digital format. The data were continuously loaded into the personal computer during the gating pulse. Ensemble averaging was performed in the PC.

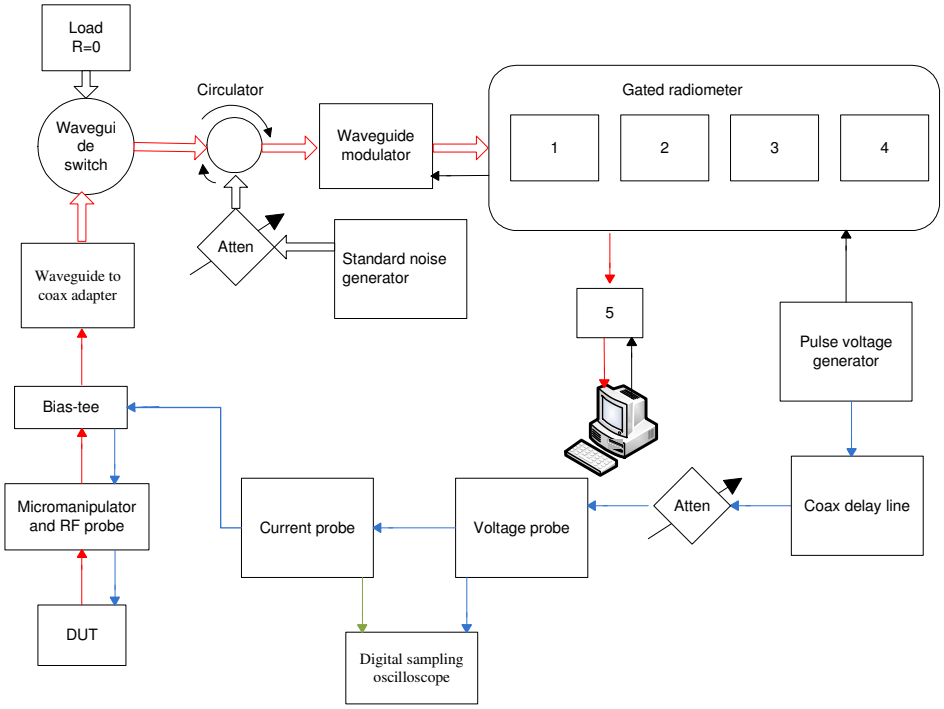

Figure 3. Waveguide-type radiometric set-up for pulsed hot-electron noise temperature measurement.

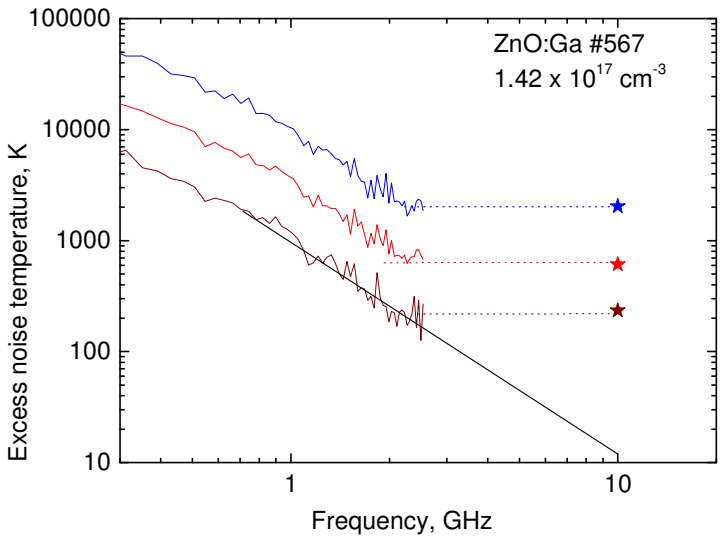

Figure 4. Noise spectra under pulsed operation at different electric fields (stars stand for X-band measurements) for sample #567: 1—22.6 kV/cm, 2—25.4 kV/cm, and 3—29 kV/cm (brown, red, and blue curves, respectively). The black line represents extrapolation, and the dotted lines are guides to the eye.[22]

The pulse repetition frequency is rather low, in the range of 100 Hz to 200 Hz. When the modulator is connected to the DUT, the integrated signal is proportional to the noise temperature of the DUT. At other times, the signal is proportional to the room temperature (noise of the matched load). Difference of the both temperatures is proportional to the excess noise temperature of the DUT. The difference is obtained when the integrated signals are subtracted in the PC. Alternating is a tricky technique which is used because it helps to rule out slow drift of the system and low-frequency 1/f fluctuations in the non-ideal components of the set-up. The standard noise generator, the coaxial short and the microwave probe calibration standards are used for the calibration purposes. The methodological equations can be found in Ref. 22.

The hot-electron noise temperature $T_n(f)$ is determined from the available noise power $\Delta P_n(f)$ emitted by the hot electrons into a matched load (input of the measurement circuit):

$$T_n(f) = \frac{1}{k_B}\frac{\Delta P_n(f)}{\Delta f} \qquad (1)$$

where k_B is the Boltzmann constant and Δf is the frequency bandwidth around the frequency f. Measurements at microwave frequencies rule out the noise sources dominant at low/moderate frequencies (Fig. 4) [22].

2.3. Estimation of Background Temperature

The thermal walkout takes place when the electrons are heated above the thermal bath temperature by the applied electric field. The hot electrons together with the hot phonons dissipate the excess heat mainly through interaction with acoustic phonons, and the latter are responsible for draining the heat out of the channel. Let us introduce the thermal bath (background) temperature T_b. different from the remote heat sink temperature T_0. The excess background temperature $\Delta T_b = T_b - T_0$ appears if the acoustic phonons are displaced from the equilibrium because of the Joule heat. The excess temperature ΔT_b can be minimized when short pulses of voltage are applied. Controlling temperature T_b is a prerequisite for investigation of excess hot-electron temperature $\Delta T_e = T_e - T_b$ as a function of electron density n.

The channel background temperature can be estimated by measuring the noise temperature as a function of time in the way described in Ref. [21]. The procedure is explained in Figure 5. Let us measure the noise temperature T_n during and after the voltage pulse. The supplied power causes an increase in the noise temperature (Fig. 5, symbols). The slow walkout is observed after the power switch off (black solid curve). Red symbols stand for channel #571 where the electron density is relatively high: $n_{3D} = 2.39 \cdot 10^{18}$ cm^{-3}. The tail is negligible in sample #567 (blue symbols, $n_{3D} = 1.42 \cdot 10^{17}$ cm^{-3}). The tail is measured in absence of supplied power; thus $T_b(t) = T_n(t)$. The back extrapolation of the exponential 'tail' (red dashed line in Figure 5) yields the background temperature of $\Delta T_b \sim 35$ K at the moment when the excess noise temperature is $\Delta T_n \sim 95$ K.

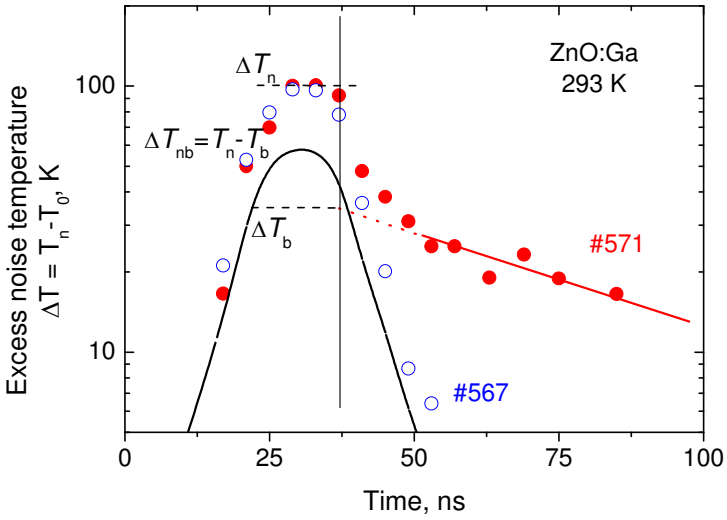

Figure 5. Time-dependent excess noise temperature measured during and after voltage pulse (pulse halfwidth is 25 ns). Symbols illustrate experimental data for two ZnO channels measured with gating pulse halfwidth of 7 ns. Black solid curve is supplied electric power due to the voltage pulse. Red solid line is an approximation; red dashed line is its extrapolation. Blue symbols are lifted up until the maxima match for comparison.

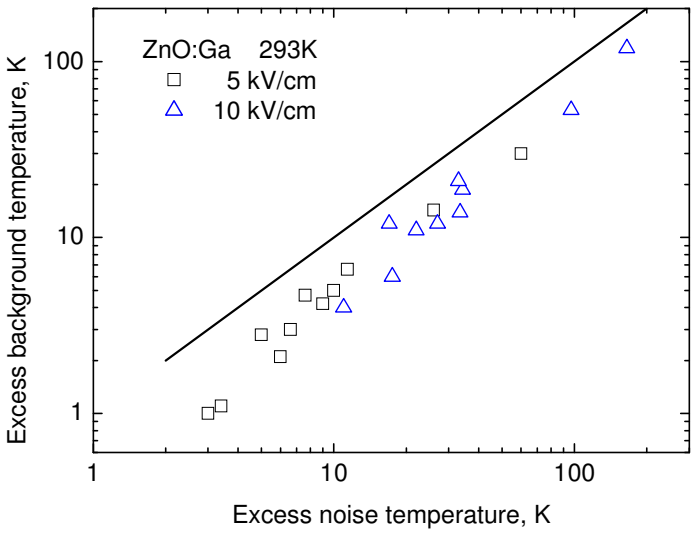

Figure 6. Estimated excess background temperature as a function of excess noise temperature for different channels subjected to the same electric field: 5 kV/cm (squares) and 10 kV/cm (triangles). Voltage pulse duration is 20 ns. Solid line is $\Delta T_b = \Delta T_n$.

Consequently, the excess hot-electron noise temperature due to the hot electrons only is $\Delta T_{eb} = T_n - T_b \sim 60$ K at the background temperature of $T_b \sim 328$ K. Of course, the noise temperature increases as

well: T_n ~ 388 K (Fig. 5 present the excess temperatures). The experimental results for different samples subjected to the same voltage pulse duration are illustrated in Figure 6 (symbols). The background temperature increases together with the hot-electron noise temperature. The hot-electron effect becomes difficult to resolve at high densities at high electric fields (triangle at right-hand-top position).

2.4. Hot-electron Energy Relaxation Time

The hot-electron energy relaxation time τ_ε enters the relation valid in the hot-electron temperature approximation [21, 24]:

$$\Delta T_{eb} = \tau_\varepsilon (2/d) P_s/k_B, \qquad (2)$$

where the excess hot-electron temperature ΔT_{eb} is estimated from the noise measurements, P_s is the electric power supplied to an average electron, d is either 2 or 3 for 2DEG and 3DEG channels, respectively.

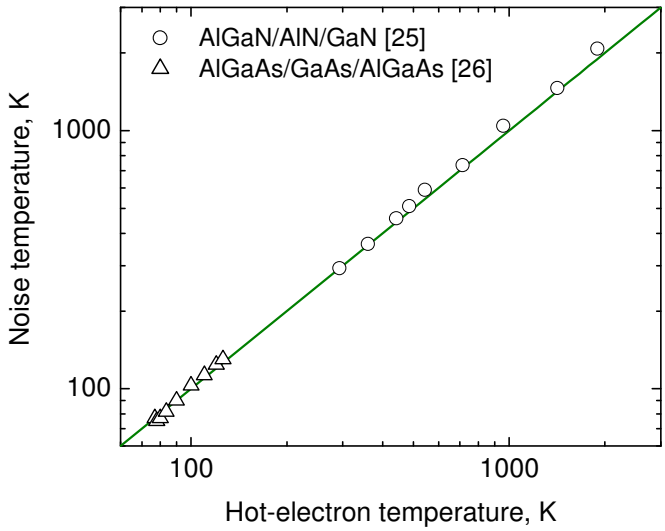

Figure 7. Calculated dependence of noise temperature on hot-electron temperature for 2DEG channels located in AlGaN/AlN/GaN at 300K (circles [25]) and AlGaAs/GaAs/AlGaAs at 77 K (open triangles [26]). Line is hot-electron temperature.

The electron temperature approach is an acceptable approximation at a high density of electrons in heavily doped and 2DEG channels of interest for FETs and HFETs. According to Monte Carlo simulation carried out for AlGaN/AlN/GaN channels, the noise temperature T_n is close to the hot-electron temperature T_e [25] (Figure 7, circles and line). A similar conclusion has been earlier reported for AlGaAs/GaAs/AlGaAs channels [26] (open triangles). Intense electron–LO-phonon interaction makes this approach also suitable for ZnO.

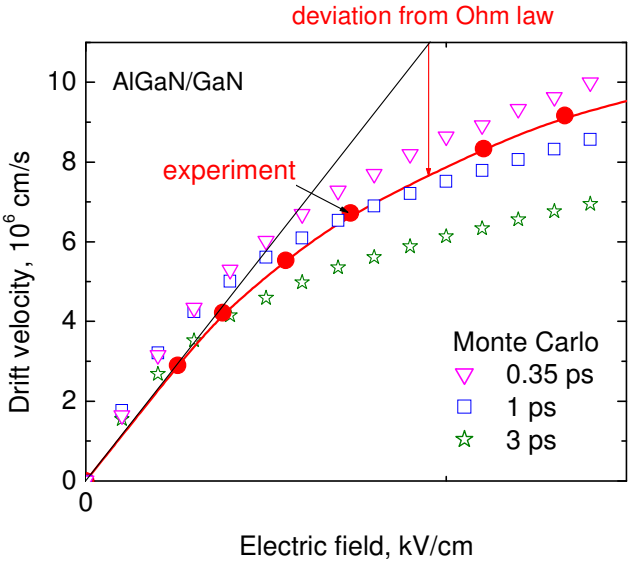

Figure 8. Deviation from the Ohm law controlled by hot-electron energy dissipation: Monte Carlo simulation (open symbols [23]) and experiment (closed symbols [27]). Black line stands for Ohm law. Red curve guides the eye.

There is another way to estimate the hot-electron energy relaxation time in voltage-biased channels. A fitting of a transport model with the measured data yields the model parameters. Figure 8 illustrates the measured hot-electron drift velocity (solid symbols) together with the results of Monte Carlo simulation (open symbols) [27]. The simulation shows that the deviation (arrow) from the Ohm law (black line) depends on the hot-phonon lifetime used in the model. A shorter hot-phonon lifetime ensures a faster relaxation of the electron energy [28]. The fitting of the experimental data with those of the simulation can be used for estimation of the electron energy relaxation time.

2.5. Monte Carlo simulations

Monte Carlo modeling is a convenient technique for considering different scattering mechanisms of the hot electrons in terms of Boltzmann kinetic equation. We have carried out ensemble Monte Carlo simulations for bulk wurtzite ZnO at 300 K thermal bath temperature. All material parameters required for the simulations are available in Ref. [30]. The electron motion and scattering in the one-valley spherical parabolic conduction band are considered. The electron effective mass m* is treated as a scalar quantity equal to 0.21 m_0 [30]. The scattering mechanisms included in the simulation are: acoustic phonon scattering, LO phonon scattering, and ionized impurity scattering. Since electron-electron interaction is efficient only at low electric fields, our model neglects an electron-electron scattering; the associated scattering rate decreases rapidly as the field increases. We treat acoustic phonon scattering as an inelastic process, because the elastic approximation might lead to an inaccurate evaluation of the energy dissipation at low–moderate electric fields. The electrons interact with the acoustic phonons both through deformation potential and electrostatic polarization. The sound velocity for bulk ZnO is taken as 6590 cm/s and mass density as 6.1 g/cm3. Due to lack of experimental data,

the deformation potential is assumed a scalar quantity of 15.0 eV [30]. The strength of acoustic scattering via piezoelectric interaction is determined by the dimensionless electromechanical coupling coefficient. The piezoelectric constants required for the calculation of electromechanical coupling coefficient are e_{33} = 1.1 C/m^2, e_{31} = -0.16 C/m^2, and e_{15} -0.31 C/m^2 [30]. The ionized impurity scattering is treated in the framework of the Brooks-Herring approach. Cubic approximation is used for the LO-phonon emission and absorption. The Fröhlich interaction uses polar optical-phonon energy of 72.9 meV[30]. The static relative dielectric permittivity is taken as 8.275 and the high-frequency relative dielectric permittivity as 4.07 [30]. The hot-electron energy relaxation time is obtained from the simulated mean excess energy and dissipated power (as noted, another technique exploits fitting of deviation from the Ohm law) . The role of different scattering mechanisms is considered.

Ensemble Monte Carlo simulation is carried out for bulk wurtzite ZnO crystals at 300 K lattice temperature. The electron motion and scattering in the one-valley spherical parabolic conduction band is considered. In the range of electric fields under investigation, electron scattering into the upper valleys is expected to be unimportant and the intervalley transfer is neglected [29, 30]. The hot-phonon effect is included in the Monte Carlo model for ZnO in a manner described previously [31]. The LO-phonon distribution is updated after each event of LO-phonon emission and absorption, and after decay of the excess LO phonons. The decay into modes of the unperturbed thermal bath is treated. The time-dependent LO-phonon distribution is calculated under the assumption of dispersionless LO phonons. The decay of excess LO phonons into other modes of the thermal bath is treated in the LO-phonon lifetime approximation, the Ridley model is used [32]. The hot-phonon lifetime of 3 ps is assumed (cf. 2.5 ps for GaN [33]). The simulation enables one to calculate the hot-electron energy relaxation time at different electron densities. The results of the Monte Carlo simulations are used to calculate the mean electron energy, electron energy autocorrelation function and electron drift velocity. The simulations are carried out at a fixed background temperature of acoustic phonons representing the thermal bath for the subsystem of hot electrons and hot phonons. As mentioned, the channel background temperature differs from the hot-electron temperature and the remote heat sink temperature.

2.6. Pulsed Transport Measurements

The nanosecond-pulsed technique [34] was applied to study high-field transport at room temperature. The high-voltage pulses were formed in an electrical circuit that consisted of a DC voltage source, a mercury-wetted relay, and a charged coaxial line. The high-voltage pulse amplitude was determined by the DC source and adjusted by power attenuators. When the coaxial line was discharged through the relay, the electric pulse reached the sample through a delay line, and the transmitted signal was fed into a 0–5 GHz bandwidth storage sampling oscilloscope through a wide-band switch, a tee, and fixed thin-film attenuators. A high-frequency gauge resistor is used for calibration. The electrical circuit can be described by a simple equivalent circuit of three resistors connected in series: the internal resistance of the generator (50 Ω), the sample resistance, and the oscilloscope input resistance (50 Ω). Therefore, the current in the channel, I, equals to $U_{osc}/50$, where U_{osc} is the registered voltage of the transmitted pulse amplitude. The electric field is estimated as $E = U - IR_c/L$ where U is the voltage drop through the sample, R_c is the total contact resistance, and L is the channel length.

The hot-electron drift velocity is determined according to the simple relation under assumption of the electron density independent of the applied electric field: $v_{dr} = I(E)/e\ n_{3D}\ w\ t$ where e is the electron charge, t is the channel thickness, w is the width of the contact pattern used, and n_{3D} is the electron 3DEG density. Samples were noted to suffer soft damage from time to time at high fields. The damage is estimated according to the change of the zero-field resistance measured before and after the high-field experiment. We ignore the results when the damage exceeds 5 %.

3. Hot-electron Drift Velocity

Pulsed technique is used to investigate dependence of current on voltage. Hot electrons and hot phonons are the main causes for non-ohmic behaviour at high electric fields when the pulses of voltage are sufficiently short. Because of strong electron–LO-phonon coupling in ZnO, emission of LO phonons by hot electrons is the preferred route for dissipation of the heat gained by the mobile electrons from the applied electric field. The dissipation of the electronic heat is partly compensated by re-absorption of the emitted LO phonons. Thus the heat is shared by the hot electrons and the hot phonons before it is converted into the heat modes able to propagate across the electrically non-conductive layers towards the remote heat sink. The bottleneck forms if the hot-phonon conversion is slow and the associated hot-phonon lifetime is long. The dependence of current on the pulse duration is associated with increase in the background temperature. Nanosecond pulses of voltage are used in order to minimize the thermal walkout. The application of 1 ns voltage pulses enabled us to measure the drift velocity at electric fields up to 150 kV/cm.

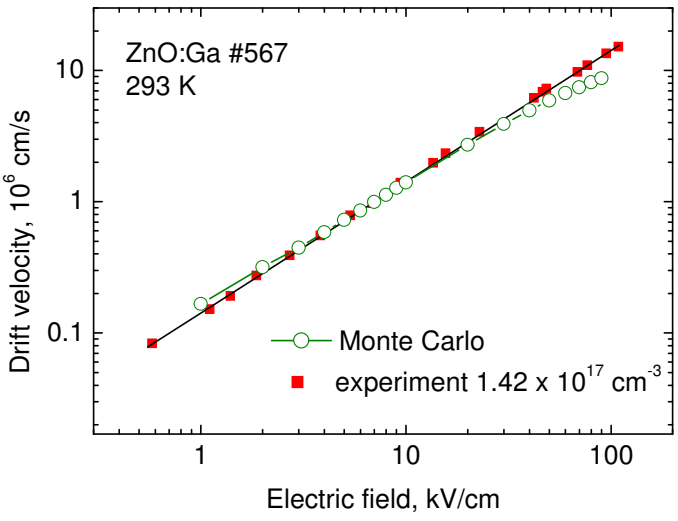

Figure 9. Dependence of drift velocity on applied electric field for sample #567 (red solid squares). Voltage pulse duration is 1 ns. Monte Carlo simulation (open circles) for hot-phonon lifetime of 1 ps.

The experimental data for sample #567 are illustrated in Figure 9 (squares). The Ohm law (black line) approximately holds at electric fields up to 100 kV/cm at the electron density of $1.42 \cdot 10^{17}$ cm^{-3} (red squares). The drift velocity is $1.5 \cdot 10^{7}$ cm/s at 104 kV/cm. This value for the drift velocity exceeds the

recently published experimental result of $7.6 \cdot 10^6$ cm/s at around 100 kV/cm at the electron density of ~$2.4 \cdot 10^{16}$ cm^{-3} measured in nominally undoped ZnO grown by MBE [35]. Sample #487 with a higher electron density of $4.6 \cdot 10^{19}$ cm^{-3} demonstrates lower values for the drift velocity (Fig. 10, red squares). The velocity is close to $3 \cdot 10^5$cm/s at 6 kV/cm for sample #487 (Fig. 10, squares) in contrast to a higher value of $8.5 \cdot 10^5$ cm/s at the same electric field for sample #567 (Fig. 9, squares).

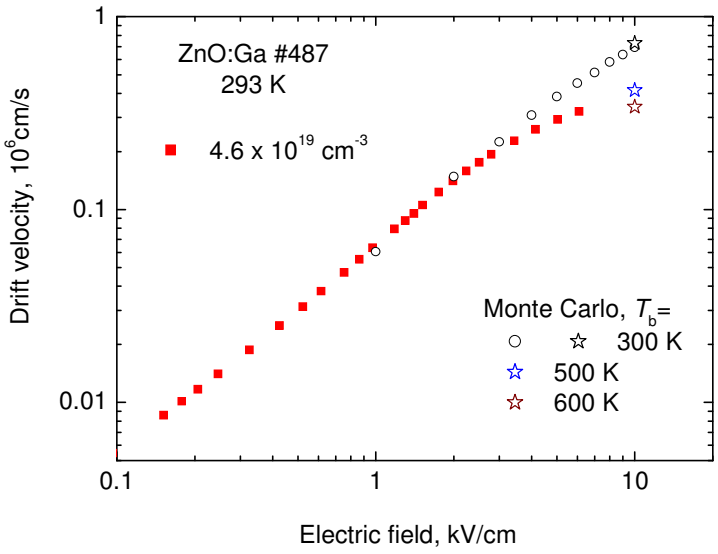

Figure 10. Dependence of drift velocity on applied electric field for sample #487 (red solid squares). Voltage pulse duration is 1 ns. Monte Carlo simulation: at room temperature for hot-phonon lifetime of 1 ps (open circles); at elevated background temperatures: 300 K (open circles and open black star), 500 K (open blue star), and 600 K (open wine star).

For ZnO the experimental electron drift velocity increases linearly with the applied electric field at electron density of $1.42 \cdot 10^{17}$ cm^{-3} (Fig. 9). This behavior fortuitously indicates a weak impact of the hot phonons on the electron transport. On the other hand, an essential deviation from the Ohm law is observed at electron density of $4.6 \cdot 10^{19}$ cm^{-3} (Fig. 10). The experimental results are compared with those of Monte Carlo simulations.

The impurity scattering is taken into account in order to fit the experimental data at low electric field. The density of impurities is artificially increased over the density of electrons—high impurity/electron density ratio is used, the compensation ratio is from 10 to 13. This is an important argument for strong elastic electron scattering in the investigated samples. Since we aim at investigation of hot-electron energy relaxation, we feel safe to mimic scattering on impurities, defects and lattice imperfections by ionized impurity scattering: the scattering on both charged and neutral lattice imperfections is usually assumed to be elastic. The results of Monte Carlo simulation are illustrated in Figures 9 and 10 under a realistic assumption that the hot-phonon lifetime is equals 1 ps (open circles and stars). The comparison with the experimental results suggests that the lifetime is below 1 ps for sample #567 (squares).

The short voltage pulses help to reduce the thermal walkout effect unless the electron density is high and the electric field is strong. Figure 10 presents the results at high electron density ($4.6 \cdot 10^{19}$ cm^{-3}) in

the electric field range below 6 kV/cm. The thermal walkout turns into the electrothermal breakdown at stronger electric fields even when the voltage pulses of 1 ns are applied. Stars in Fig. 10 illustrate the simulated hot-electron drift velocity at different background temperatures.. The drift velocity decreases as the background temperature increases. Therefore, the experimental deviation from the Ohm law cannot be interpreted in terms hot-electron energy relaxation. An interpretation in terms of elevated background temperature seems quite probable (cf. closed square and wine star in Figure 10). The alternative interpretation of the experimental data in terms of hot-phonon lifetime requires unrealistically long lifetimes—significantly longer than 1 ps—if the thermal walkout is ignored.

In conclusion, heavy impurity scattering masks the hot-electron energy relaxation effects, and the energy relaxation time is not extracted from non-ohmic transport in doped ZnO. The alternative technique for estimating the hot-electron energy relaxation time is based on noise experiment and the balance of supplied–dissipated power. The power supplied to an average electron is available from the product of the electron velocity and the electric field.

3. Doping-dependent Excess Noise

Figure 11 shows the excess noise temperature T_n-T_0 against the supplied power per electron P_e for the doped ZnO channels with different electron density (symbols). A linear dependence is an acceptable approximation (lines).

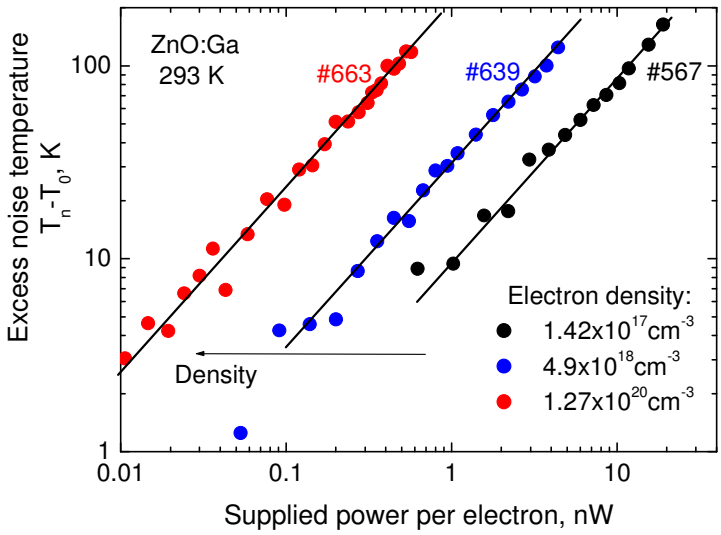

Figure 11. Dependence of excess noise temperature on supplied power per electron. Symbols stand for samples #567 (black), # 639 (blue), and #663 (red). Black lines stand for linear dependence.

The slope of the lines depends on the electron density, as illustrated in Figure 12. A non-monotonous dependence on the electron density is evident. In particular, the local minimum is observed in the

electron density range from $4.9 \cdot 10^{18}$ cm^{-3} to $1.74 \cdot 10^{19}$ cm^{-3}. Note, that the plasmon–LO-phonon resonance is expected at $6.8 \cdot 10^{18}$ cm^{-3} in bulk ZnO (as it will be explained in details later).

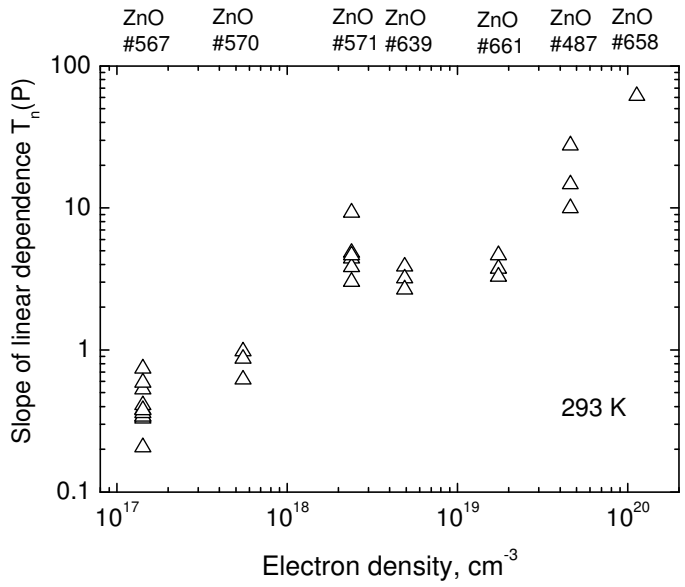

Figure 12. Slope of power-dependent excess noise temperature for samples taken from several wafers (numbers, top scale). Voltage pulse duration is 2.7 μs.

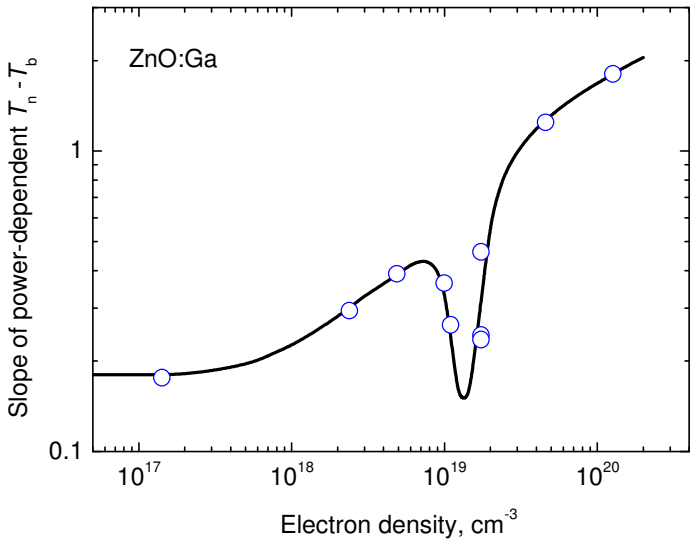

Figure 13. Density-dependent slope of power-dependent excess noise temperature over background temperature (symbols). Black curve guides the eye.

The thermal walkout effect (at the end of the pulse) is proportional to the product of voltage pulse width and the supplied power density per unit volume $P_V \sim n_{3D} \bullet P_e$ where n_{3D} is the electron density and P_e is the supplied power per electron. The latter can be found from the product of the electric field and the electron drift velocity. Thus, by keeping the same supplied power per electron and comparing devices with different electron densities, we conclude that the thermal walkout effect increases with the electron density. Even 100 ns pulses of voltage appear to be too long to avoid the thermal walkout at the highest electron densities. After the procedure illustrated in Figure 6, the net difference T_n-T_b is obtained for each channel.

The local minimum is better resolved after the following improvements. We select high quality channels and average the results of interest in order to increase the accuracy and confidence in our data. High contact quality is needed for negligible contact-related noise sources of no interest for our goals. Accordingly, some devices have been excluded from the analysis. The final noise measurements are performed for voltage pulse widths of 20 ns. The excess noise temperature over the background temperature, T_n-T_b, is obtained through the procedure described in subsection 2.3. The slope of the linear dependence of T_n-T_b on the supplied power P is obtained for channels with different electron density. The results on the slope are summarized in Figure 13 (open circles). The fitted curve demonstrates a sharp minimum near electron density of $1.4 \bullet 10^{19}$ cm^{-3}.

4. Hot-electron Energy Relaxation

4.1 Experimental Data

The hot-electron noise measurements yield the hot-electron energy relaxation time according to Eq. (2) under several conditions. The excess noise temperature is measured as a function of the supplied electric power per electron. The latter can be found from the either the product of the electric field and the electron drift velocity or the product of the current and voltage divided by the electron number in the channel. Since the deviation from the Ohm law is weak in the doped ZnO samples (Figure 9), the standard technique is not applicable for estimation of the relaxation time from the non-linearity of the current–voltage characteristic. The noise is measured in the range of electric field where the Ohm law holds, and the energy relaxation time is independent of the supplied power. In the other words, the energy relaxation time is obtained from the slope of the linear dependence on the supplied power of the excess hot-electron temperature (obtained from the noise measurements). The pulsed measurements are preferred over DC measurements in order to minimize the thermal walkout effect. After Eq. (2) the difference $T_e - T_b$ is needed for estimation of the energy relaxation time. We make it sure that the G – R and 1/f sources of noise are weak at microwave frequencies (Figure 4). The noise *spectra* measurements are used if any suspicion arises regarding the origin of the excess noise. The excess noise temperature T_n is measured at the elevated background temperature T_b; the latter is estimated in the way discussed in subsection 2.3 and Figure 5. This procedure is inevitable at high electron densities when thermal walkout comes into play. We suppose that the excess hot-electron temperature $T_e - T_b$ approximately equals the excess noise temperature $T_n - T_b$ (Figure 7).

Figure 14 summarizes available results on the energy relaxation time measured for ZnO by different techniques. A systematic dependence on electron density is difficult to resolve from the results measured by photoexcitation techniques (bullets) [8-20]. Our results [22] lead to a non-monotonous

increase of the relaxation time with the electron density (open circles). The relaxation is fast (~0.17 ps) at electron density of $1.42 \cdot 10^{17}$ cm^{-3} and reaches ~1.8 ps at the highest electron density of $1.3 \cdot 10^{20}$ cm^{-3}. The fitted curve demonstrates a sharp minimum near electron density of $1.4 \cdot 10^{19}$ cm^{-3}.

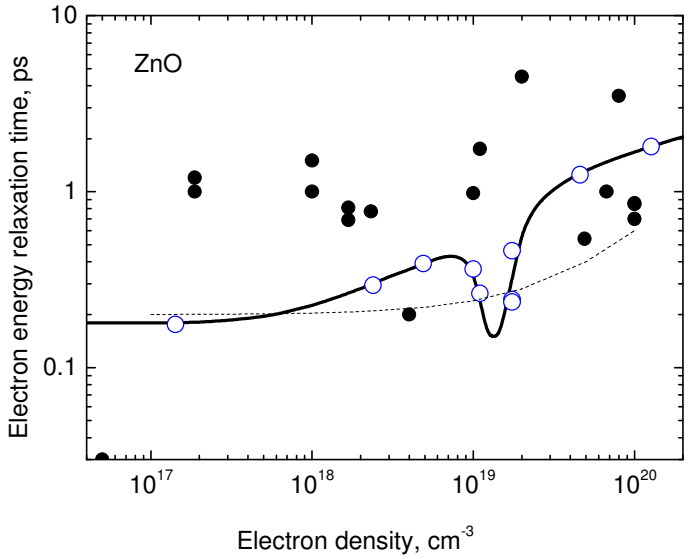

Figure 14. Hot-electron energy relaxation time for ZnO. Blue circles – present project [22], bullets – worldwide results measured by photoexcitation techniques [8-20]. Dotted curve is semi-empirical dependence [36]. Solid curve guides the eye.

The optical data are scattered in the range from 0.03 ps to 1.75 ps for different ZnO samples films, nanorods, nanowire, crystal, etc.). There should be some cause for the electron energy relaxation rate to be so different for the same material (ZnO). It is unlikely that the variation originates from the different techniques because most of the data are available from direct optical time-resolved pump–probe measurements where the reliability is high and variation is of rather secondary importance. However, a high optical power is needed to generate a high electron density. As hot electrons cool down by emitting LO phonons, the accumulated phonons slow the electron energy relaxation when the electrons reabsorb the emitted phonons. This effect is evidenced by a steep increase of the energy relaxation time from 0.2 ps to 1.75 ps as the carrier density increases from $4 \cdot 10^{18}$ cm^{-3} to $1.1 \cdot 10^{19}$ cm^{-3} [13]; the longer relaxation time has been measured at the higher pumping fluence (corresponding to a higher density of the photoexcited carriers). Ou et al. [20] also state that the carrier thermalization time increases when hot phonons come into play. The semi-empirical dependence (Figure 14, dotted curve) also suggests a slower relaxation at a higher density [36]. However, more correlation with the carrier density is difficult to discern.

4.2 Main Paths of Hot-electron Energy Relaxation

The experimental data (Fig. 15, open circles) can be fitted with the black curve. The latter can be decomposed into two curves (red and blue) representing two concurrent paths, τ_1 and τ_2, for the energy relaxation (inset, paths 1 and 2):

$$\tau_\varepsilon^{-1}=\tau_1^{-1}+\tau_2^{-1}. \quad (3)$$

Path A (inset) stands for direct interaction of electrons with background acoustic phonons. For simplicity, we ignore path A. Indeed, the acoustic scattering is quasi-elastic and causes very long energy relaxation time which is of minor importance for the discussion. The electron–LO-phonon coupling is relatively strong in polar semiconductors. This scattering prevails over the acoustic phonon scattering even at room temperature.

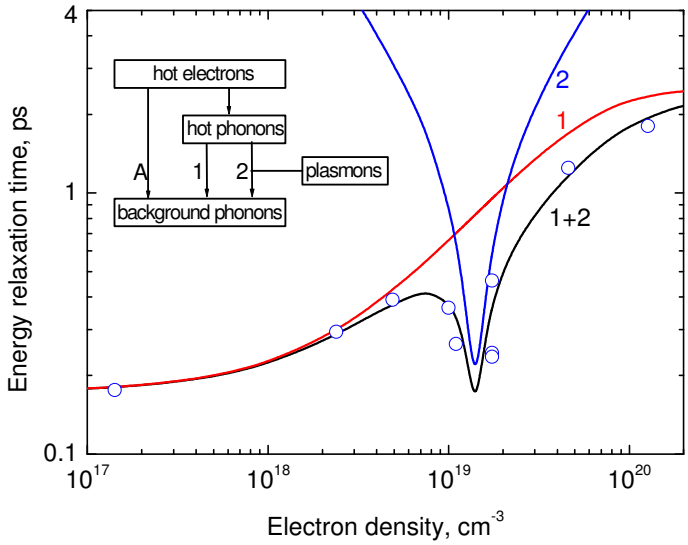

Figure 15. Dependence of hot-electron energy relaxation time on electron density for doped ZnO. Red line (path 1) is Eq. (4), blue line (path 2) is Eq. (5). Black line is Eq. (3) for the combined effect (paths 1 and 2) . Inset illustrates paths for hot-electron energy relaxation [22].

The relaxation along the first path (indicated with numeral 1, Fig. 15) is approximated by a monotonous dependence on density (red curve)

$$\tau_1 = a_1\,(1-\exp(-n_{3D}/n_1)+b_1), \quad (4)$$

while the resonance curve (blue) stands for

$$\tau_2 = a_2\{1+ b_2\,(n_{3D}/n_2-n_2/n_{3D})^2\}^{1/2}. \quad (5)$$

Here a_1, a_2, b_1, b_2, n_1 and n_2 are the fitting constants. The physical origin of the paths is worthwhile to discuss.

The hot LO phonons (emitted by the hot electrons and accumulated in the channel) can decay into longitudinal acoustic phonons and transverse optical phonons, likely through the Ridley path (path 1) [32]. Path 2 assumes plasmon-assisted decay of hot phonons. This path has been earlier resolved in experiments on GaN [33] and 2DEG channels for heterostructure field effect transistors [31]. Black curve in Figure 15 illustrates the combined effect of paths 1 and 2 and fits the experimental data reasonably well (Fig. 15, blue open circles). Further discussion of paths 1 and 2 includes Monte Carlo simulation of electron scattering.

4.3 Monte Carlo: Effect of Equilibrium LO Phonons

Monte Carlo modeling is a convenient technique for considering different scattering mechanisms of hot electrons in terms of the Boltzmann kinetic equation. The details of Monte Carlo procedure are given in subsection 2.5.

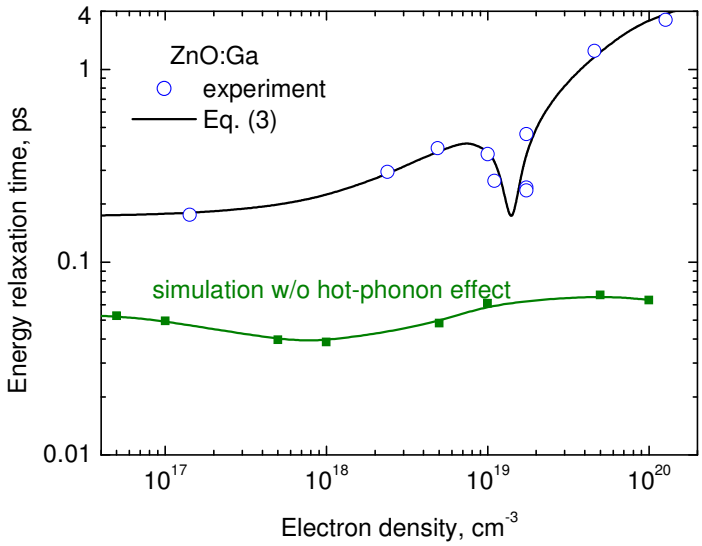

Figure 16. Monte Carlo simulation of hot-electron energy relaxation time for doped ZnO when hot-phonon effect is ignored (green symbols and curve). Blue circles are experimental data. Black line is Eq. (3) for the combined effect (paths 1 and 2).

Squares in Fig. 16 represent the density dependence of the electron energy relaxation time obtained by the Monte Carlo simulation under the assumption that the LO-phonon distribution is kept unchanged, that is, the emitted LO phonons are not added to the equilibrium distribution. The calculated energy relaxation time is nearly independent of the electron and impurity density (squares). In this way, the insignificant role of impurity scattering is demonstrated: the impurity scattering is strong but elastic, and thus it has no direct effect on the energy relaxation. No agreement with black line (paths 1 and 2) is obtained if hot phonons are ignored.

5. Hot-phonon Effect

5.1 Monte Carlo: Density-independent Hot-phonon Lifetime

To reiterate, the hot electrons dissipate their excess energy predominately through interaction with LO phonons. The non-equilibrium LO phonons (hot phonons) play an essential role in dissipation. This can be demonstrated through calculations of hot-electron energy autocorrelation function. The autocorrelation function results from fluctuations in electron energy and illustrates electron energy relaxation.

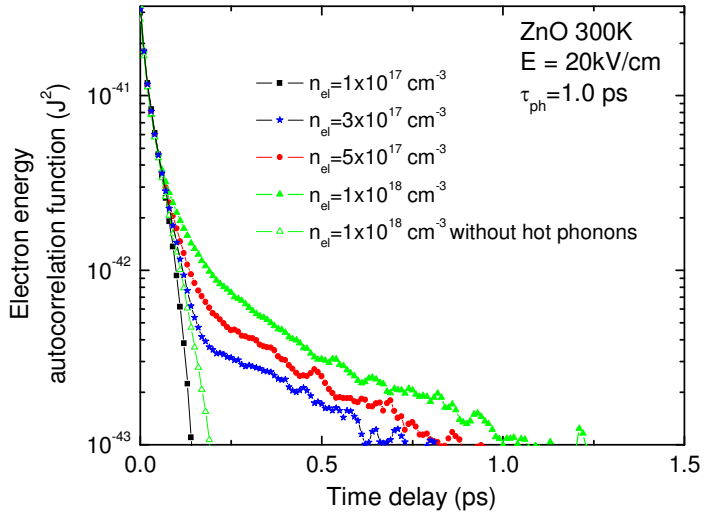

Figure 17. Dependence of electron energy autocorrelation function on the time delay. Closed symbols represent the Monte Carlo data with hot-phonon effect at different electron gas density: $1 \cdot 10^{17}$ cm^{-3} (black squares), $3 \cdot 10^{17}$ cm^{-3} (blue stars), $5 \cdot 10^{17}$ cm^{-3} (red circles), $1 \cdot 10^{18}$ cm^{-3} (green triangles). Open triangles ignore hot phonon effect when the Monte Carlo simulation is performed for electron gas density of $1 \cdot 10^{18}$ cm^{-3}.

The time-dependent autocorrelation function is obtained from ensemble Monte Carlo simulation. The results are shown in Figure 17 for four different values of electron gas density: $1 \cdot 10^{17}$ cm^{-3} (black squares), $3 \cdot 10^{17}$ cm^{-3} (blue stars), $5 \cdot 10^{17}$ cm^{-3} (red circles), $1 \cdot 10^{18}$ cm^{-3} (green triangles). The initial ultrafast decay of the autocorrelation function is followed by a longer tail.

The tail is caused by the hot phonons as confirmed through a comparison of the results simulated for electron gas density of $1 \cdot 10^{18}$ cm^{-3} with and without hot-phonon effect (solid triangles and open triangles, correspondingly). While the results show almost no hot-phonon effect on the initial ultrafast relaxation, the tail demonstrates a strong effect caused by hot phonons. Within the accuracy of Monte Carlo simulation, the tail of the electron energy autocorrelation function is not resolved at an electron gas density of $1 \cdot 10^{17}$ cm^{-3} (Fig. 17, closed black squares)—the hot-phonon effect is weak at this density. The tail qualitatively corresponds to the relaxation of the coupled electron–LO-phonon subsystem due to its interaction with external bodies: acoustic phonons, etc.

Circles in Figure 18 present the results of Monte Carlo calculations performed under assumption of constant hot-phonon lifetime (τ_{ph}= 3 ps). The hot-electron energy relaxation becomes slower at higher electron gas density (Fig. 18, circles). The Monte Carlo results are in a qualitative agreement with red curve in Figure 15.

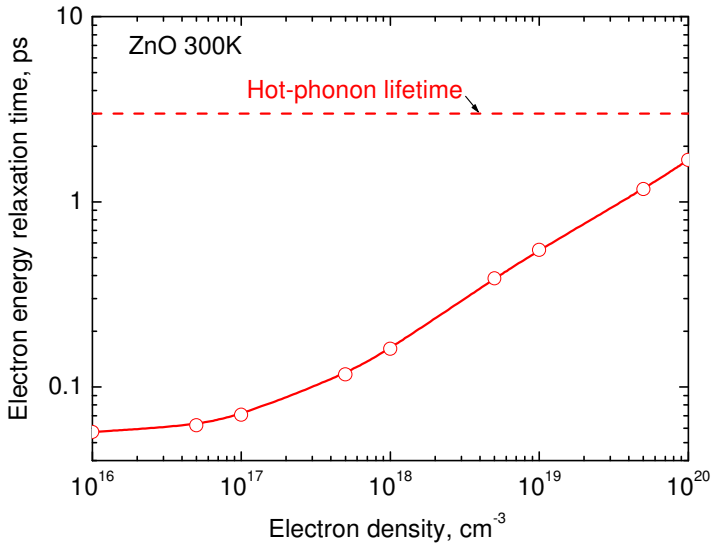

Figure 18. Monte Carlo simulation of density-dependent hot-electron energy relaxation time for doped ZnO. Open circles represent Monte Carlo data with hot-phonon effect taken into account (τ_{ph}= 3 ps is assumed, dashed line). Solid curve guides the eye.

5.2. Coupling Index of Hot-electron and Hot-phonon Gases

According to the simulation the occupancy of hot-phonon modes increases together with the electron density provided that the same electric power per electron is supplied. As a result, the coupling of the hot-electron gas with the hot-phonon gas increases. The both hot gases tend to relax together at high densities—in other words, the electron energy relaxation time tends to the hot-phonon lifetime.

Let us introduce the index of coupling as follows:

$$\beta = \tau_{\varepsilon}/\tau_{ph} \, . \qquad (6)$$

The index β is low in at low densities and tends to unity when the gases become dense (Figure 19). The transition of the hot-electron–hot-phonon system from the weak coupling regime to the intense coupling regime is evidenced.

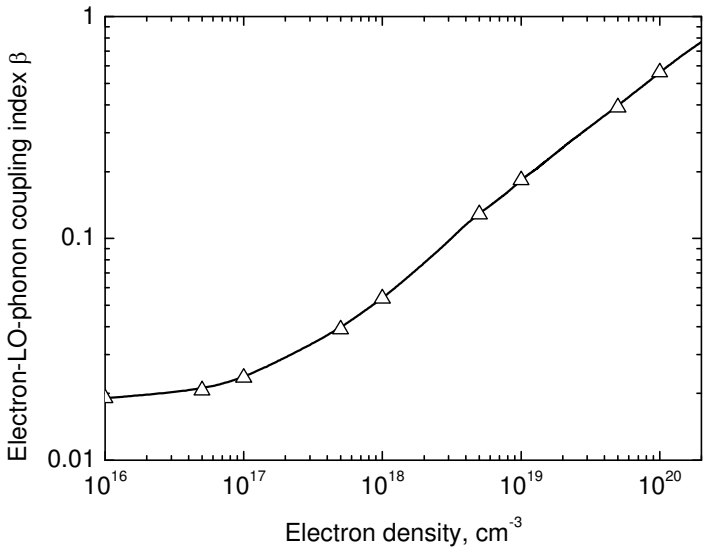

Figure 19. Coupling index of hot-electron and hot-phonon gases.

The definition of coupling index given by Eq. (6) and the data of Figure 19 allow one to extract hot-phonon lifetime from the experimental data on the hot-electron energy (Fig.14, blue circles).

5.3. Density-dependent Hot-phonon Lifetime

The experimental data of Fig.14 (open circles) together with the results of simulation presented in Fig. 19 yield the experimental-based dependence of the hot-phonon lifetime on the electron density illustrated in Figure 20 (green stars). Two features are evident: (i) the fast decay of hot phonons takes place in the vicinity of the resonance electron density of $1.4 \bullet 10^{19}$ cm^{-3}, (ii) the hot-phonon lifetime is (3±0.5) ps far away from the resonance.

Figure 21 compares the obtained results for doped ZnO (red circles) with those obtained from time-resolved pump–probe Raman experiments for nominally undoped GaN [33]. The carrier density is controlled by the pulsed photexcitation in the GaN. The lifetime for GaN at 'low' density (10^{16} cm^{-3}) is ~2.5 ps. This value is comparable with the estimated off-resonance hot-phonon lifetime for ZnO (~3 ps). The lifetime for ZnO (green squares) decreases as the resonance is approached. This finding is in a qualitative agreement with the results for GaN (black squares) at sub-resonance densities. The result is interpreted within the model of coupled plasmon–LO-phonon modes (black line, [37]). The results for ZnO (green stars) are obtained for a wide range of the densities, that is, below and above the resonance (green stars). A similar resonance for LO phonons has not been reported for doped bulk semiconductors.

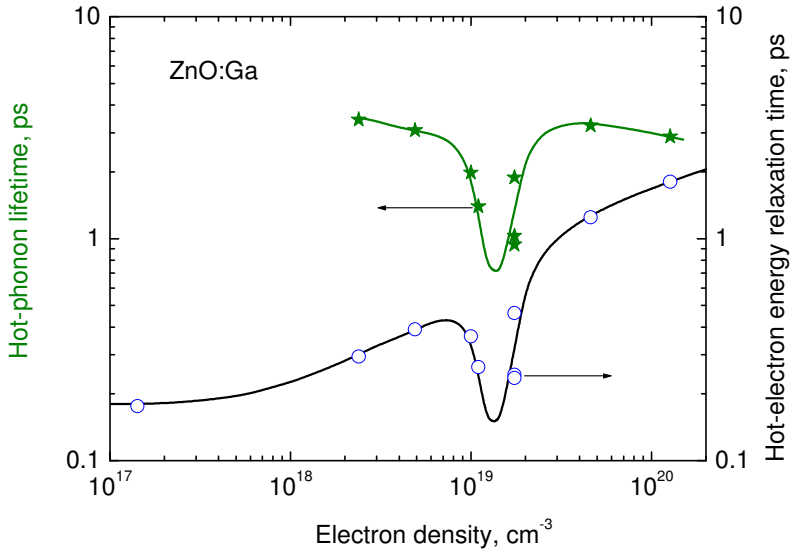

Figure 20. Experimental dependence of hot-phonon lifetime on electron density for doped ZnO at room temperature (green symbols). Blue symbols stand for hot-electron energy relaxation time. Lines guide the eye.

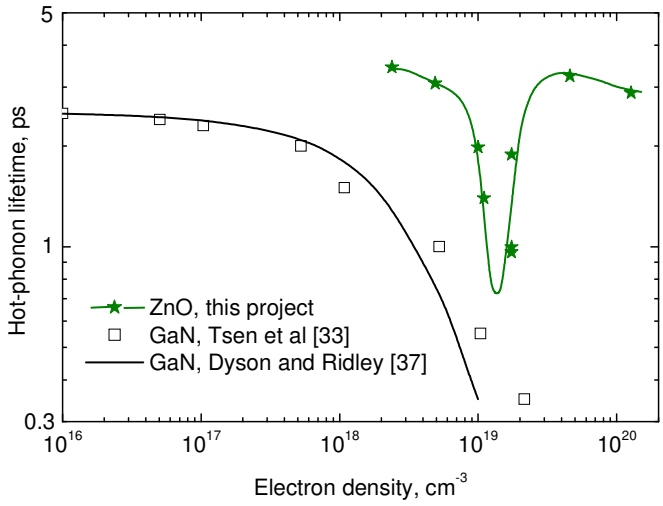

Figure 21. Experimental dependence of hot-phonon lifetime on electron density for doped ZnO (green stars, present project) and nominally undoped GaN (black squares, [33]). Black line stands for theoretic model of decay of coupled plasmon–LO-phonon modes [37]. Green line guides the eye.

5.4. Resonance Enhancement of Hot-electron Drift Velocity

The enhanced resonance decay of hot phonons has a direct consequence on various phenomena where the excess occupancy of hot-phonon modes plays an important role [5-7]. In particular, the electron scattering by the non-equilibrium excess (hot) phonons is weaker if the occupancy of the involved hot-phonon modes is lower. This can be demonstrated by measuring the hot-electron drift velocity in various samples at the chosen value of applied electric field. Typically, the effect is masked by the Joule effect: the increase in background temperature causes a stronger scattering of electron by acoustic phonons. The Joule effect is important at high electric field in channels with high electron density. Application of short pulses of voltage allows one to reduce the thermal walkout effect dramatically. .

Figure 22 illustrates the results on the drift velocity measured for channels with different electron density subjected to short pulses (1.5 ns) of voltage.

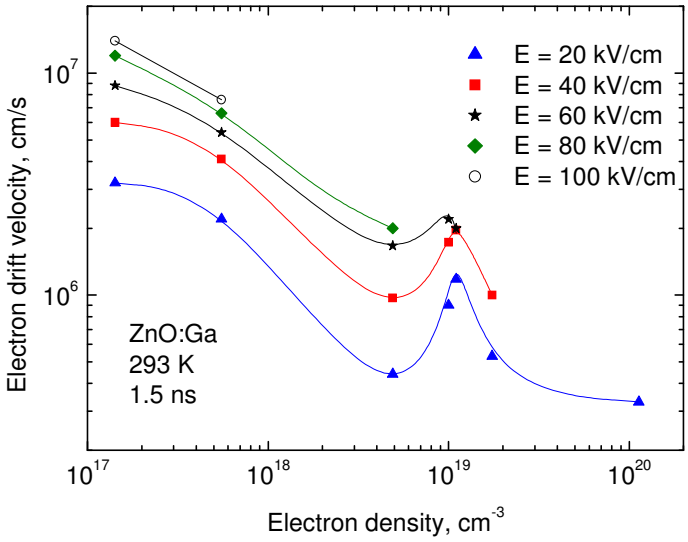

Figure 22. Experimental dependence of hot-electron drift velocity on electron density for doped ZnO (symbols, present project). Lines guide the eye. Data at high fields for high-density channels are missing because of thermal runaway. Voltage pulse duration 1.5 ns.

Typically, the drift velocity decreases if the doping increases. This happens in the electron density range from $1 \cdot 10^{17}$ cm^{-3} to $5 \cdot 10^{18}$ cm^{-3} for doped ZnO (Fig.22, symbols). The velocity stops decreasing at around $5 \cdot 10^{18}$ cm^{-3}, and the local maximum forms at higher densities at intermediate electric fields in the range from 20 kV/cm to 60 kV/cm (triangles, squares, stars). The thermal runaway makes it impossible to resolve the maximum at electric fields of 80 kV/cm and 100 kV/cm (diamonds, circles). The maximum is located at above 10^{19} cm^{-3}. Its position (Fig. 22) correlates with that of the resonance decay of hot phonons (Fig. 21). Thus, the observed fast decay of hot phonons supports high values of hot-electron drift velocity unless the thermal runaway comes into play.

6. Ultrafast Decay of Hot Phonons in 2DEG Channels

The dependence of hot-phonon lifetime on electron density suggests participation of plasmons as confirmed by the modeling (Fig. 21, blue curve, [37]). Plasmons take part in dissipation of the heat accumulated in the hot-electron–hot-phonon system (Fig. 15, inset, path 2). The fastest relaxation of the hot-electron energy is expected at (and in the vicinity) of the resonance where the strongest coupling takes place among the plasmons and the LO-phonons. As mentioned, this phenomenon is useful for microwave electronics [6]: the plasmons pave the way for the electron density window where the ultrafast dissipation of electron energy supports operation of transistor channels at the highest frequency with the slowest channel degradation [5,7]. The fast decay of hot-phonons can be associated with the plasmon–LO-phonon resonance.

For an infinite uniform electron plasma, the frequency ω_{PL} of an uncoupled mode of plasmon approaches that of an LO phonon at the 3DEG electron density

$$n_{cr} = \omega_{LO}^2 \frac{m^* \varepsilon}{e^2} \quad , \tag{7}$$

where ω_{LO} is the LO-phonon frequency at zero electron density, m^* is the electron effective mass and ε is the dielectric constant. After Eq. (7), the frequency crossover electron density is $6.8 \cdot 10^{18}$ cm^{-3} in ZnO. The plasmon–LO-phonon coupling is expected to become most important in the vicinity of the crossover density. The experiment shows that the resonance is resolved at a higher density (Fig. 20). The resonance shift towards higher density is interpreted as a consequence of reduced plasmon frequency in thin conductive channels.

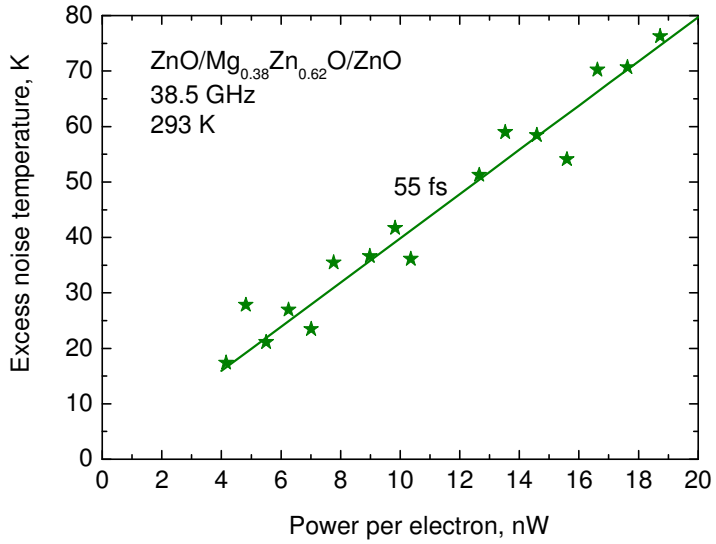

Figure 23. Dependence of excess hot-electron noise for 2DEG channel located in $ZnO/Mg_{0.38}Zn_{0.62}O/ZnO$ structure. Line is drawn for τ_{ph} = 55 fs. [23]

An additional confirmation of the plasmon-assisted decay of hot phonons is obtained through experimental investigation of 2DEG channels. The 2DEG channels for HFETs contain high density electron gas. According to solution of the Schroedinger–Poisson equations and capacitance–voltage measurements, typical values reach and exceed 10^{20} cm^{-3} in GaN-based heterostructures [7]. As a result, the hot-electron temperature approximately equals the hot-phonon temperature (Fig. 7), and they relax together. We assume that the hot-electron energy relaxation time approaches the hot-phonon lifetime (Fig. 18), and a measurement of the former yields the latter.

Figure 23 presents the power dependence of excess hot-electron noise measured for $ZnO/Mg_{0.38}Zn_{0.62}O/ZnO$ structure at 38.5 GHz frequency. The set-up is operated at this frequency in order to suppress the source of G–R noise important at 10 GHz and lower frequencies. The experimental data (Fig. 23, stars) are fitted with Eq. (2) (line), and $\tau_\varepsilon = 55$ fs is extracted. As discussed, the approximate equality of τ_ε and τ_{ph} holds for 2DEG channels used in HFETs.

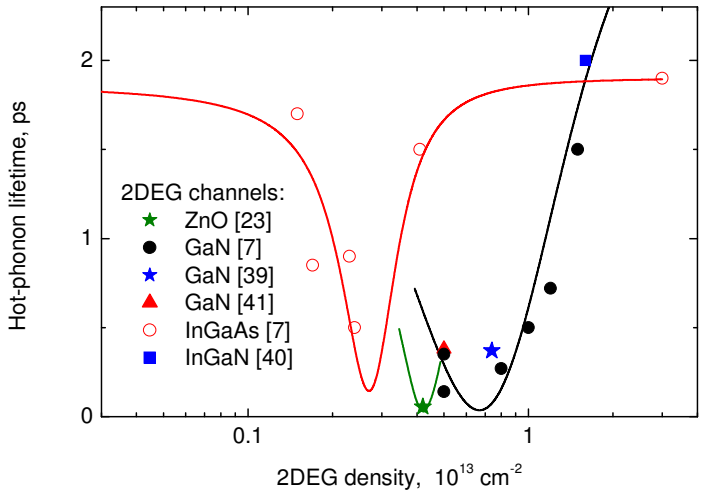

Figure 24. Hot-phonon lifetime in 2DEG channels located in $ZnO/Mg_{0.38}Zn_{0.62}O/ZnO$ structure (green star, present project) together with the data for 2DEG channels confined in GaN (black bullets [7], blue star [39], red triangle [41]), InGaAs (red circles [7]) and InGaN (blue square [40]). Solid curves illustrate Eq. (5).

The obtained hot-phonon lifetime for the ZnO/MgZnO/ZnO (Fig. 24, green star) is the shortest among the results presented in Fig. 24. The associated ultrafast decay is a strong indication that the 2DEG density of $5.5 \cdot 10^{12}$ cm^{-2} is close to the resonance density. In particular, the relaxation time (green star) is two times shorter than the shortes LO-phonon lifetime in the GaN 2DEG channel (black bullets).

Because of large conduction band gap in MgZnO, the 2DEG is predominantly located in the top ZnO layer at the ZnO/MgZnO interface of the ZnO/MgZnO/ZnO structure. The LO-phonon energy in ZnO is lower than that in GaN (72meV and 92 meV, respectively). Correspondingly, the 2DEG density in the ZnO channel (green star, Fig. 24) is lower as compared with the resonance density for GaN 2DEG

layers (black bullets, Fig. 24) in a qualitative agreement with Eq. (7). Solid curves in Fig. 24 fit the experimental data and demonstrate that the resonance electron densities are different for red (InGaAs), green (ZnO) and black (GaN) curves in correlation with the LO phonon energies in the corresponding 2DEG channels. The difference may be understood by invoking a simple model, which equates the plasmon energy to that of the LO phonon. The plasmon energy depends on the plasma wavelength in thin plasma layers and tends to the value in uniform infinite plasma as the wavelength becomes shorter. The wavelengths of the emitted LO phonons are short. The resonance density for the investigated $ZnO/Mg_{0.38}Zn_{0.62}O/ZnO$ structure finds itself in between those for arsenides and nitrides as expected from their relation with the plasmon–LO-phonon resonance.

The ultrafast energy relaxation in the ZnO 2DEG channels is demonstrated for relatively low power per electron (the data are presented for 4 nW per electron). The measurements above 20 nW are limited by onset of thermal walkout and residual effect of the field on the channel resistance. We demonstrate that the hot-electron energy relaxation is quite fast at the selected electron density. However, we do not know how sharp is the resonance. There is always a statistical variation in the electron density in the wafer. In particular, each open circle in the Figure 20 is an average over several devices having nominally the same electron density though the actual density differs. Because of the statistical averaging the fitting curve is less sharp than the reonance one.

Let us compare the resonance density for the ZnO 2DEG channel with the that for doped ZnO films where the hot-phonon lifetime is estimated over a wide range of 3DEG densities (Fig. 21). The comparison is not straigtforward because the 3DEG density is not constant in the 2DEG channel; it depends on the position in the transverse direction. The density profile resembles a rather asymmetrical Gauss function, and only some average 3DEG density can be specified for the 2DEG channel. Consider the approach where the thickness of the channel is estimated as the width of the density profile at the Fermi level. Typical thickness values are several nanometers. Taking a realistic value between 3 nm and 5 nm for the 2DEG channel in question, we get the average 3DEG density between $1.8 \cdot 10^{19}$ cm^{-3} and $1.1 \cdot 10^{19}$ cm^{-3}. This range includes the experimental value for the 3DEG channels in doped ZnO ($1.4 \cdot 10^{19}$ cm^{-3} ,Fig. 21).

Main Results and Conclusions

The hot-electron transport, noise, and energy relaxation were investigated in the donor-doped bulk wurtzite ZnO (epitaxial layer form) and the ZnO/$Mg_{0.38}Zn_{0.62}O$/ZnO structure with a two-dimensional electron gas (2DEG) subjected to a strong electric field. The Ga-doped and Sb-doped gateless ZnO channels contained electron density in the range from $1.4 \cdot 10^{17}$ cm^{-3} to $1.3 \cdot 10^{20}$ cm^{-3}. The electron sheet density in the 2DEG channel was $5.5 \cdot 10^{12}$ cm^{-2}. The non-equilibrium longitudinal optical phonons (hot phonons) were found to play an essenetial role. The plasmon-assisted decay of hot phonons supported an enhanced electron drift velocity, fast relaxation of electron energy, and reduced hot-electron noise in the electron density window located in the vicinity of plasmon–LO-phonon resonance.

The spectral measurements of noise confirmed that frequency-dependent noise sources dominate over the hot-electron noise in the frequency range from 0.2 GHz to 2.5 GHz. The hot-electron noise was studied in the X and Ka bands. The results were treated in terms of hot-electron temperature and hot-electron energy relaxation time. The relaxation time increased from 0.17 ps to 1.8 ps when the electron density increased from $1.4 \cdot 10^{17}$ cm^{-3} to $1.3 \cdot 10^{20}$ cm^{-3}. The local minimum is resolved near the electron density of $1.4 \cdot 10^{19}$ cm^{-3}. A systematic dependence of the relaxation time on the electron density is measured for the donor-doped ZnO for the first time.

Monte Carlo simulations provided with a qualitative interpretation of the observations when accumulation of hot phonons was taken into account. The transition of the hot-electron–hot-phonon system from the weak coupling regime to the intense coupling regime was evidenced. The results of Monte Carlo simulations for density-independent hot-phonon lifetime were in a qualitative agreement with the experimental data, except for the local minimum resolved at the electron density of $1.4 \cdot 10^{19}$ cm^{-3}. The local minimum was associated with the plasmon-assisted rapid decay of hot phonons as demonstrated earlier for nitride and arsenide two-dimensional channels.

Nanosecond pulsed measurements yielded hot-electron drift velocity in agreement with those of Monte Carlo simulation when the density of the ionized impurities was assumed to exceed that of the electrons by 10–13 times. The Ohm law approximately held in the electric field range up to 100 kV/cm at electron density of $1.42 \cdot 10^{17}$ cm^{-3}. The highest value for the drift velocity of $1.5 \cdot 10^{7}$ cm/s was measured at 104 kV/cm field. The non-ohmic behavior was mainly caused by thermal walkout at high electron densities.

The hot-electron noise measurements at a 38.5 GHz frequency demonstrated an ultrafast relaxation of hot-electron energy in the 2DEG channel confined in ZnO/$Mg_{0.38}Zn_{0.62}O$/ZnO structure. The relaxation time of 55 fs was extracted at a 2DEG density of $5.5 \cdot 10^{12}$ cm^{-2}. The ultrafast relaxation occured in the vicinity of LO-phonon–plasmon resonance. The comparative analysis of the results for 2DEG channels located in ZnO, GaN, InGaN, and InGaAs supported the conclusion that the heat dissipation by hot phonons is enhanced by plasmons. The result for the 2DEG channel was in good agreement with those obtained for the doped ZnO films.

The experimental investigation of fluctuations provided a wealth of information on fast processes affecting high-field performance of doped ZnO channels for FETs and HFETs. The hot-electron velocity fluctuations measured at a microwave frequency were used for resolving the electron density window for the fastest relaxation of hot-electron energy and high values of drift velocity at a high electron density. The main results can be summarized as follows:

1. The hot-electron energy relaxation time is measured for the donor-doped ZnO channels subjected to the pulsed electric field applied in the channel plane.
2. The measured hot-electron energy relaxation time presents a systematic non-monotonous dependence on electron density in the range from $1.4 \cdot 10^{17}$ cm^{-3} to $1.3 \cdot 10^{20}$ cm^{-3}.
3. The transition of the hot-electron–hot-phonon system from the weak coupling regime to the intense coupling regime is evidenced.
4. The minima of hot-electron energy relaxation time and hot-phonon lifetime are resolved at the electron density of $1.4 \cdot 10^{19} cm^{-3}$ in the donor-doped ZnO.
5. The ultrafast relaxation is observed at the sheet density of $5.5 \cdot 10^{12}$ cm^{-2} in the 2DEG channel confined in the $ZnO/Mg_{0.38}Zn_{0.62}O/ZnO$ structure.
6. The experimental results are interpreted in terms of the two-path model of the electron energy relaxation through the traditional interaction with hot phonons plus the resonance plasmon-assisted hot-phonon decay.
7. The non-monotonous dependence of the hot-electron drift velocity on the electron density is measured for the doped ZnO channels at high electric fields. The local maximum (resolved at the electron density of $1.4 \cdot 10^{19}$ cm^{-3} in the donor-doped ZnO channels) correlates with the minimum of the hot-phonon lifetime.
8. The electron drift velocity of $1.5 \cdot 10^{7}$ cm/s is measured at electric field of 104 kV/cm in Ga-doped ZnO channels at electron density of $1.42 \cdot 10^{17}$ cm^{-3}.
9. The electron density window is resolved in the vicinity of the plasmon–LO-phonon resonance. The lowest hot-electron noise, the fastest energy relaxation, the fastest decay of hot phonons, and the highest product of drift velocity with electron density are demonstrated inside the window.

In conclusion, the ZnO 3DEG and 2DEG channels can be operated at the electron density window where the energy relaxation is faster, the noise is lower, and the electron drift velocity is enhanced as compared with the same values at the off-window electron densities. Models based on Boltzmann kinetic equation for hot electrons fail to interpret the experimental results unless hot-phonon accumulation is taken into account and the problem is treated in terms of the coupled kinetic equations for hot electrons and hot phonons. The assumption of electron density-independent hot-phonon lifetime explains the transition of the hot-electron–hot-phonon system from the weak coupling regime to the intense coupling regime but fails to predict the position of the window. The plasmon-assisted ultrafast decay of hot phonons is the main cause for the resolved density window.

References

[1] S. Pearton, Ed., *GaN and ZnO-based Materials and Devices: Springer Series in Materials Science*. Berlin, Heidelberg:Springer-Verlag, 2012, vol. 156

[2] H. Morkoç and Ü. Özgür, *Zinc Oxide: Fundamentals, Materials and Device Technology*, Wiley-VCH, Berlin, 2009

[3] V. Avrutin, G. Cantwell, J. Zhang, J. J. Song, D. Silversmith, and H. Morkoç, Bulk ZnO: Current Status, Challenges, and Prospects, *Proceedings of IEEE* **98**, 1269 (2010)

[4] H. Liu, V. Avrutin, N. Izyumskaya, Ü. Özgür, and H. Morkoç, *Superlattices Microstruct.* 48, 458 (2010).

[5] A. Matulionis, J. Liberis, E. Šermukšnis, L. Ardaravičius, A. Šimukovič, C. Kayis, C. Y. Zhu, R. Ferreyra, V. Avrutin, Ü. Özgür, and H. Morkoç, *Microelectron. Reliab.* **52**, 2149 (2012).

[6] A. Matulionis, J. Liberis, I. Matulionienė, M. Ramonas, and E. Šermukšnis, Ultrafast removal of LO-mode heat from a GaN-based two-dimensional channel, *Proceedings of IEEE* **98**, 1118 (2010)

[7] A. Matulionis, Electron density window for best frequency performance, lowest phase noise and slowest degradation of GaN heterostructure field-effect transistors, *Semiconductor Science and Technology* **28** 074007 (2013)

[8] A. Yamamoto, T. Kido, T. Goto, Y. Chen, T. Yao and A. Kasuya, "Dynamics of photoexcited carriers in ZnO epitaxial thin films," *Appl. Phys. Lett.*, vol. 75, no. 4, p. 469, 1999.

[9] J. Takeda, H. Jinnouchi, S. Kurita, Y. F. Chen and T. Yao, "Dynamics of photoexcited high density carriers in ZnO epitaxial thin films," *Phys. Stat. Sol. B*, vol. 229, no. 2, p. 877, 2002.

[10] J. Takeda, "Femtosecond Dynamics of Photoexcited High Density Carriers in ZnO Epitaxial Thin Films," *Nonlinear Optics*, vol. 29, p. 521, 2002.

[11] Y. Toshine, J. Takeda, H. J. Ko, and T. Yao, "Conversion of an electronhole plasma into a high density excitonic state in ZnO epitaxial thin films," *Phys. Stat. Sol. C*, vol. 1, no. 4, p. 839, 2004.

[12] C. Li, D. Feng, T. Jia, H. Sun, X. Li, S. Xu, X. Wang and Z. Xu, "Ultrafast dynamics in ZnO thin films irradiated by femtosecond lasers," *Sol. State Comm.*, vol. 136, p. 389, 2005.

[13] C.K. Sun, S.Z. Sun, K.H. Lin, K.Y.J. Zhang, H.L. Liu, S.C. Liu and J.J. Wu, "Ultrafast carrier dynamics in ZnO nanorods," *Appl. Phys. Lett.*, vol. 87, p. 023106, 2005.

[14] N. Arai, J. Takeda, H-Ju. Ko and T. Yao, "Dynamics of high-density excitons and electron-hole plasma in ZnO epitaxial thin films," *J. Luminescence*, vol. 119-120, p. 346, 2006.

[15] J. Takeda, N. Arai, Y. Toshine, Hang-Ju. Ko and T. Yao, "Ultrafast dynamics of exciton-exciton and exciton-longitudinal optical-phonon scattering processes in ZnO epitaxial thin films," *Jpn. J. Appl. Phys.*, vol. 45, no. 9A, p. 6961, 2006.

[16] X.M. Wen, J.A. Davis, D. McDonald, L.V. Dao, P. Hannaford, V.A. Coleman, H.H. Tan, C. Jagadish, K. Koike, S. Sasa, M. Inoue and M. Yano, "Ultrafast dynamics in ZnO/ZnMgO multiple quantum wells," *Nanotechnology*, vol. 18, no. 31, p. 315403, 2007.

[17] W.A. Tisdale, M. Muntwiler, D.J. Norris, E.S. Aydil, and X.-Y. Zhu, "Electron dynamics at the ZnO (101-0) surface," *J. Phys. Chem. C*, vol. 112, p. 14682, 2008.

[18] P. C. Ou, J. H. Lin, C. A. Chang, W. R. Liu and W. F. Hsieh, "Thickness effect on ultrafast thermalization of carriers in above-band-gap states in ZnO epitaxial films," *J. Phys. D: Appl. Phys.*, vol. 43, no. 49, p. 495103, 2010.

[19] P. C. Ou, W. R. Liu, H. J. Ton, J. H. Lin and W. F. Hsieh, "Ultrafast relaxation and absorption saturation at near exciton resonance in a thin ZnO epilayer," *J. Appl. Phys.*, vol. 109, p. 013102, 2011.

[20] P.C. Ou, J.H. Lin and W.F. Hsieh, "Spectral dependence of transient reflectance in a ZnO epitaxial film at room temperature," *Appl. Phys. B*, vol. 106, p. 399, 2012.

[21] H.L. Hartnagel, R. Katilius, and A. Matulionis, *Microwave Noise in Semiconductor Devices* (Wiley, New York, 2001).

[22] E. Šermukšnis, J. Liberis, M. Ramonas, A. Matulionis, M. Toporkov, H. Y. Liu, V. Avrutin, Ü. Özgür, and H. Morkoç "Hot-electron energy relaxation time in Ga-doped ZnO films", *Journal of Applied Physics* **117**, 065704 (2015)

[23] E. Šermukšnis, J. Liberis A. Matulionis, M. Toporkov, V. Avrutin, Ü. Özgür, H. Morkoç, Hot-electron noise and energy relaxation in wurtzite ZnO *Proceedings of ICNF* **23**, 1570080493 (2015)

[24] A. Matulionis and I. Matulionienė, "Hot-electron noise in III-V semiconductor structures for ultra-fast devices"in: *Noise and Fluctuations Control in Electronic Devices*, edited by A. A. Balandin (American Scientific Publishers, Stevenson Ranch, 2002), pp. 249–266.

[25] A. Matulionis, J. Liberis, and M. Ramonas, **"**Microwave noise in biased AlGaN/GaN and AlGaN/AlN/GaN channels" *American Institute of Physics Conference Proceedings* **CP780** 105–108 (2005)

[26] X.L. Lei and N.J.M. Horing, "Thermal noise temperature of GaAs heterosystems for steady-state hot-electron transport with nonequilibrium phonons," *Physical Review* **B 36** 4238–4248 (1987).

[27] A. Matulionis, J. Liberis, I. Matulionienė, M. Ramonas, L.F. Eastman, J.R. Shealy, V. Tilak, and A. Vertiatchikh, "Hot-phonon temperature and lifetime in a biased $Al_xGa_{1-x}N$/GaN channel estimated from noise analysis," *Physical Review* **B 68** 035338/1-7 (2003).

[28] A. Matulionis, "Hot phonons in GaN channels for HEMTs"*Physica Status Solidi(A) Applications and Materials* **203**(10) 2313–2325 (2006).

[29] J. Liberis, M. Ramonas, O. Kiprijanovič, A. Matulionis, N. Goel, J. Simon, K. Wang, H. Xing and D. Jena, "Hot phonons in Si-doped GaN," *Appl. Phys. Lett.*, vol. 89, p. 202117, 2006.

[30] E. Furno, F. Bertazzi, M. Goano, G. Ghione and E. Bellotti, "Hydrodynamic transport parameters of wurtzite ZnO from analytic- and fullband Monte Carlo simulation," *Solid-State Electronics*, vol. 52, p. 1796, 2008.

[31] M. Ramonas, A. Matulionis, J. Liberis, L. Eastman, X. Chen, and Y. -J. Sun, "Hot-phonon effect on power dissipation in a biased AlxGa1xN/AlN/GaN channel," *Phys. Rev. B*, vol. 71, p. 075324, 2005.

[32] B. K. Ridley, *J. Phys.: Condens. Matter* **8,** L511 (1996).

[33] K. T. Tsen, J. G. Kiang, D. K. Ferry, and H. Morkoç, *Appl. Phys. Lett***. 89**, 112111 (2006).

[34] L. Ardaravičius, A. Matulionis, J. Liberis, O. Kiprijanovič, M. Ramonas, L.F. Eastman, J.R. Shealy, and A. Vertiatchikh, "Drift velocity in AlGaN/GaN at high electric fields", *Appl.Phys. Lett.*, **83**, 4038 (2003).

[35] S. Sasa, T. Maitani, Y. Furuya, T. Amano, K. Koike, M. Yano, and M. Inoue, "Microwave performance of ZnO/ZnMgO heterostructure field effect transistors", *Phys. Status Solidi* A **208**, 449 (2011).

[36] M. A. M. Versteegh, T. Kuis, H. T. C. Stoof, and J. I. Dijkhuis, *Phys. Rev.B* **84**, 035207 (2011).

[37] A. Dyson and B.K. Ridley, Phonon–plasmon coupled-mode lifetime in semiconductors, *J. Appl. Phys.* **103**, 114507 (2008)

[38] A. Matulionis, GaN-based two-dimensional channels: hot-electron fluctuations and dissipation, *Journal of Physics: Condensed Matter* **21**, 174203 (2009)

[39] J. Liberis, M. Ramonas, E. Šermukšnis, P. Sakalas, N. Szabo, M. Schuster, A. Wachowiak, A. Matulionis, Hot-phonon lifetime in $Al_{0.23}Ga_{0.77}N$/GaN channels, *Semiconductor Science and Technology* **29**(4), 045018 (2014)

[40] L. Ardaravičius, O. Kiprijanovič, J. Liberis, E. Šermukšnis, A.Matulionis, R. A. Ferreyra, V. Avrutin, Ü. Özgür, H. Morkoç, Threshold field for soft damage and electron drift velocity in InGaN two-dimensional channels, *Semiconductor Science and Technology* (2015) (accepted)

[41] Z. Wang, K. Reimann, M. Woerner, T. Elsaesser, D. Hofstetter, J. Hwang, W.J. Schaff, and L.F. Eastman, Optical phonon sidebands of electronic intersubband absorption in strongly polar semiconductor heterostructures, *Phys. Rev. Lett.* **94**, 037403 (2005).

List of Symbols, Abbreviations, and Acronyms

FET – field-effect transistor
MESFET – metal-semiconductor field-effect transistor
HFET – hetereostructure field effect transistor
2DEG – two-dimensional electron gas
2DEG density – electron sheet density
3DEG – three-dimensional electron gas
3DEG density – electron density per unit volume
DC – direct current
RF – radio frequency (microwave included)
X-band – microwave frequency band near 10 GHz
Ka band – microwave frequency band near 38 GHz
cut-off frequency – unity gain frequency
millimeter-wave frequencies – above30 GHz, below 300 GHz
X-ray diffraction – diffraction of Roentgen rays
Fröhlich interaction is the electron–LO-phonon interaction
JCA812 – microwave low noise amplifier
SR250 – gated integrator and boxcar averager module (Stanford Research Systems)
SR240A – quad fast amplifier (Stanford Research Systems)
SR245 – computer interface module (Stanford Research Systems)
RS232 – interface module
Labview – computer software
PC – personal computer
TLM – transmission line method
DUT – device under test
GHz = 10^9 Hz
PMBE – plasma-enhanced molecular beam epitaxy
heterojunction – monocrystallic interface of two semiconductors with different bandgap
heterostructure – monocrystallic structure that contains one or more heterojunctions
LA phonons – longitudinal acoustic phonons
LO phonons – longitudinal optical phonons
LO-mode heat – heat accumulated by non-equilibrium LO phonons
hot electrons – non-equilibrium high-temperature electrons
hot phonons – LO phonons launched by hot electrons
hot-phonon lifetime – time constant for conversion of hot phonons into migrant modes
plasmons – quanta of collective vibrations of electron gas
plasmon–LO-phonon crossover means that plasmon energy equals LO-phonon energy
thermal walkout – time-dependent variation of measurables caused by device self-heating
ultrafast <100 fs
f is the frequency
Δf is the frequency bandwidth
$\hbar\omega_{LO}$ is the LO-phonon energy
$\hbar\omega_{PL}$ is the plasmon energy
I is the current

k_B is the Boltzmann constant
L is the channel length
w is the channel width
d is the channel thickness
n_{2D} is the 2DEG density
n_{3D} is the 3DEG density
n_{cr} is the plasmon–LO-phonon crossover electron density
ε is the dielectric constant
e is the elementary (electron) charge
E is the electric field strength
e_{33} , e_{31} , e_{15} are the electromechanical coupling coefficients
m^* is the electron effective mass
m_0 is the electron mass
$\Delta P_n(f)$ is the available noise power
P_e is the dissipated power per electron
P_s is the supplied electric power per electron
P_v is the supplied electric power per unit volume
R_c is the contact resistance
$T_n(f)$ is the hot-electron noise temperature
T_e is the hot-electron temperature
T_{LO} is the hot-phonon temperature
T_b is the channel background temperature
T_0 is the equilibrium temperature (heat sink temperature)
τ_{ph} is the hot-phonon lifetime
τ_ε is the hot-electron energy (temperature) relaxation time
v_{dr} is the electron drift velocity
U is the applied voltage
U_{osc} is the transmitted voltage pulse amplitude registered by oscilloscope
ZnO is zinc oxide
$Mg_{0.38}Zn_{0.62}O$ is the mixed crystal of ZnO and MgO
Ga – donor in ZnO
InGaN– mixed crystal of GaN and InN
InGaAs– mixed crystal of GaAs and InAs
ICNF – International Conference on Noise and Fluctuations
IWZnO– International Workshop on Zinc Oxide and related Materials
VCU– Virginia Commonwealth University